5-2024

RSM for the Optimization of Selective Laser Melting Process Parameters for Manufacturing Initial Layers of Horizontal Overhang Structures

Prince Yaw Asamani
The University of Texas Rio Grande Valley

RSM FOR THE OPTIMIZATION OF SELECTIVE LASER MELTING PROCESS PARAMETERS FOR MANUFACTURING INITIAL LAYERS OF HORIZONTAL OVERHANG STRUCTURES

A Thesis

by

PRINCE YAW ASAMANI

Submitted in Partial Fulfillment of the

Requirements for the Degree of

MASTER OF SCIENCE IN ENGINEERING

Major Subject: Manufacturing Engineering

The University of Texas Rio Grande Valley

May 2024

RSM FOR THE OPTIMIZATION OF SELECTIVE LASER MELTING PROCESS PARAMETERS FOR MANUFACTURING INITIAL LAYERS OF HORIZONTAL OVERHANG STRUCTURES

A Thesis
by
PRINCE YAW ASAMANI

COMMITTEE MEMBERS

Dr. Benjamin Peters
Chair of Committee

Dr. Jianzhi Li
Committee Member

Dr. Douglas Timmer
Committee Member

May 2024

ABSTRACT

Asamani, Prince Y., RSM for The Optimization of Selective Laser Melting Process Parameters for Manufacturing Initial Layers of Horizontal Overhang Structures. Master of Science in Engineering (MSE), May 2024, 42 pp., 5 tables, 66 figures, 35 references.

While prevalent in 3D printed objects, overhang features are difficult to print with selective laser melting due to the limitation of a purely vertical laser. To address this issue, overhang features are typically built on temporary supports, which are removed following printing. However, this results in wasted material and longer production time. Several authors have studied printing overhangs without support structures. However, there has not been a systematic approach to studying the effect of multiple process parameters on the quality of a printed overhang. This thesis investigates the effect of laser power, scanning speed, and hatch distance on the surface area of the initial layers of a horizontal overhang structure. By optimizing the surface area of the initial layers, we create a solid foundation upon which subsequent layers can be successfully built.

DEDICATION

I dedicate this work to my cherished friends and family, whose unwavering love, encouragement, and support have been the cornerstone of my academic pursuits, fueling my determination throughout.

ACKNOWLEDGEMENTS

I am deeply grateful to Dr. Benjamin Peters, my thesis committee chair, for his invaluable mentorship, guidance, and unwavering support throughout my academic journey. His profound insights and encouragement have been instrumental in shaping my research endeavors. I am also thankful to Dr. Jianzhi Li and Dr. Douglas Timmer for their advice, patience, and direction on my project, which have been pivotal in ensuring its successful completion.

TABLE OF CONTENTS

LIST OF TABLES

LIST OF FIGURES

CHAPTER I

INTRODUCTION

Selective Laser Melting (SLM) is a form of additive manufacturing that utilizes a high-intensity laser to melt and join specific areas of powder layer by layer, based on computer-aided design (CAD) information (Osakada & Shiomi, 2006; Yap et al., 2015). The ability of SLM to produce parts with intricate geometries without limitations associated with traditional methods has made it popular and widely adopted across diverse industries, including aerospace, automobile, and medical fields (Gu et al., 2020).

As the SLM additive manufacturing technology progresses, novel challenges emerge, including the imperative for support structures during the printing process. These structures play a crucial role in securing components on a substrate material, thereby enhancing heat conduction throughout the SLM process (Hussein, Hao, Yan, & Everson, 2013). A persistent issue within this context is the production of horizontal overhang structures, where the absence of support structures can lead to problems like balling, warping, and spattering, which can result in processing failures. To mitigate these issues, support structures are strategically placed (Shi et al., 2019; Vasileska et al., 2022; D. Wang et al., 2013). However, these structures are considered waste materials, resulting in increased usage of powder material, longer production times, and more post-processing (Hussein, Hao, Yan, Everson, et al., 2013; K. Zhang et al., 2018).

A good amount of literature exists on optimizing support structures for printing horizontal overhang structures. However, the literature for the optimization of process parameters for SLM of supportless overhang structures is limited and thus our motivation for expanding on this body of knowledge. This study aims to investigate the relationship between the process parameters and the surface area of the initial layers. These layers are printed directly on powder without support, for selective laser melted supportless overhang structures.

Research Questions

This research aims to investigate and optimize the process parameters for the SLM additive manufacturing of initial layers of horizontal overhang structures without the need for support structures. For this research, we investigate the research questions as presented below:

1. What is the relationship between the process parameters and the surface area of the initial layers of selective laser melted supportless overhang structures?
2. How does the surface area of the initial layers affect selective laser melted horizontal supportless overhang structures?
3. What are the effects of directly printing on powder?

CHAPTER II

LITERATURE REVIEW

Selective Laser Melting (SLM) is a form of additive manufacturing that utilizes a high-intensity laser to melt and join specific areas of powder to form parts. After achieving the appropriate cross-section for one layer, the powder bed is lowered by a predetermined layer thickness, and a new layer of powder is evenly dispersed across it. The process is repeated until the part is complete (Osakada & Shiomi, 2006; Yap et al., 2015). To prevent oxidation when printing, the build chamber is filled with an inert gas, typically argon or nitrogen (Canacoo, 2022; Ferrar et al., 2012).

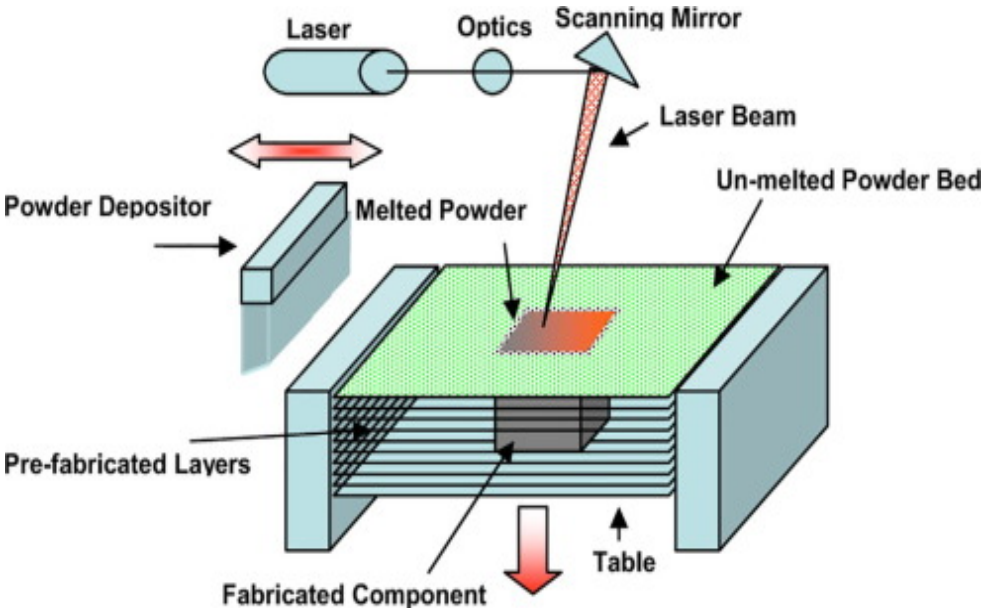

Figure 1: SLM process as illustrated by Mumtaz et al. (Chua & Leong, 2014)

The use of SLM to fabricate horizontal overhang structures is difficult due to the limitation of purely vertical laser. During the SLM process, prefabricated layers act as support for the current layer being printed. Printing directly on powder without a support structure causes defects which include balling, spattering, and warping (Shi et al., 2019; D. Wang et al., 2013; Z. Yuan & Chen, 2023).

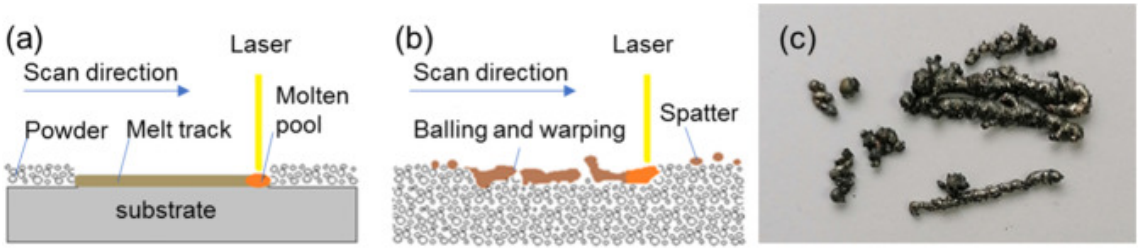

Figure 2: Balling, warping and spattering effect a) printing on substrate b) printing directly on powder c) photograph of the results of balling effect (Yuan & Chen, 2023)

.

A typical solution for fabricating horizontal overhang structures would be to employ support structures that play a crucial role in securing the part unto the substrate and enhancing heat conduction during the process. However, support structures are considered waste materials, resulting in increased usage of powder material, longer production times, and more post-processing (Hussein, Hao, Yan, Everson, et al., 2013; K. Zhang et al., 2018). This makes the fabrication of horizontal overhang structures a challenge.

Research in the field has explored various strategies to overcome the difficulties associated with creating horizontal overhang structures. Fox et al. studied the effect of beam power, beam velocity, and overhang angle on the surface roughness parameter of the overhang surface using EOS M 270. Samples were printed parallelepipeds at overhang angle $\alpha = 30°, 45°, 60°,$ and $75°$. The results from the analysis of surface roughness parameters suggested that reducing

the overhang angle increases average roughness (Ra), mean width (RSm), mean height (Rc) while Peak count (Rpc) reduces (Fox et al., 2016).

Yuan et al. proposed a new strategy for the fabrication of overhangs by utilizing a defocused laser beam during the initial layer printing process. In this study, two cubes were printed adjacent to each other on a build platform using standard printing parameters. Following this, three horizontal overhanging layers, measuring 8 mm × 40 mm, were added on top. Sample 1 was printed with a defocused laser and lower scan speed, sample 2 with reduced laser power and scan speed, while sample 3 followed normal parameters. The hatch spacing for all samples was set to 65 µm. Despite slight variations, all three samples had similar linear energy densities: 400 J/s for samples 1 and 2, and 367 J/s for sample 3. Micrographs and 3D images of the upper surface of the samples depicted in Figure 5 reveal the challenge of successfully printing on a powder bed without a substrate using a focused laser beam under conventional conditions. However, utilizing a defocused laser beam allowed for the creation of branch-like layers with strong mechanical integrity and flatness (Z. Yuan & Chen, 2023).

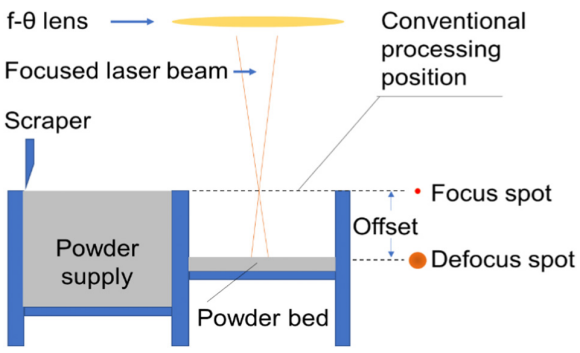

Figure 3: Schematic diagram of the control of the laser spot size by means of the powder bed offset parameter (Z. Yuan & Chen, 2023).

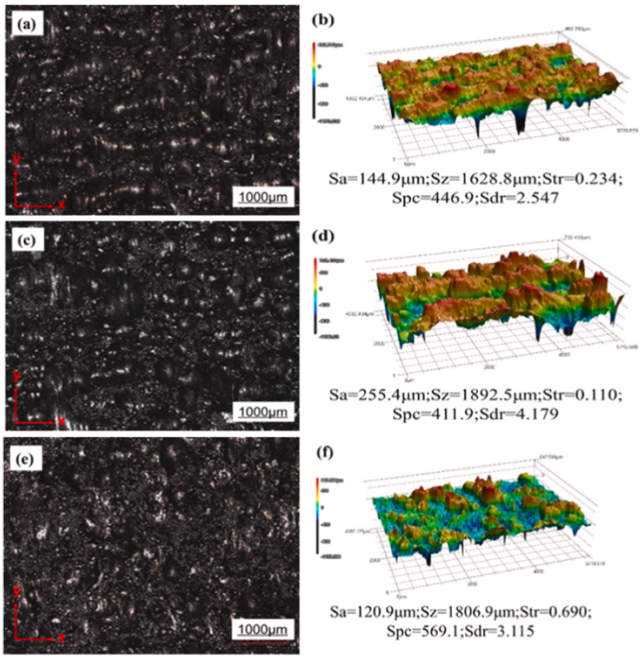

Figure 4: Micrograph and 3D images of Samples (Z. Yuan & Chen, 2023)

Yuan et al. conducted a study utilizing a second-order model to explore the impact of laser power, scanning speed, and powder thickness on overhang thickness. The experimental design adhered to the principles of the Box-Behnken Design (BBD). Laser power, scanning speed, and layer thickness were identified as key factors, with the objective of achieving a 1 mm overhang thickness. It's noteworthy that once the overhang thickness reaches 1 mm, subsequent printing layers have minimal influence on the sagging and concavity of the overhang surface, hence justifying the selection of 1 mm as the target function (Z. Yuan & Chen, 2023). The results from the analysis show that an optimal overhang thickness of 1.37mm was achieved at Laser power 200W, a scanning speed of 998mm/s, and powder thickness at 45μm (M. Yuan et al., 2024).

Several researchers have investigated the areas of support design (Hussein, Hao, Yan, & Everson, 2013; Malians et al., 2016; Sundar et al., 2014; Y. Wang et al., 2020), structural design (Fox et al., 2016; D. Wang et al., 2016), support removal (Hildreth et al., 2016; Lefky et al., 2017),

numerical simulation analysis ((Chen et al., 2017; He et al., 2019; Hodge et al., 2016; Khairallah & Anderson, 2014; Markl & Körner, 2016), process control (Carter et al., 2014), quality control (Atzeni & Salmi, 2015; Jiang et al., 2020; Sun et al., 2017; D. Wang et al., 2016), and scanning strategy (Cheng et al., 2016; Kruth et al., 2012; Zaeh & Branner, 2010; X. Zhang et al., 2018).

This thesis proposes a response surface methodology to identify the optimal SLM printing parameters that maximize the surface area filled by printing the initial layer of a horizontal overhang structure. By optimizing the surface area of the initial layer, a good layer that serves as substrate for subsequent layers is formed.

.

CHAPTER III

RESPONSE SURFACE METHODOLOGY

This experiment was performed to determine the optimal parameters for printing the initial layers of supportless overhang structures. Response surface methodology was employed for this study.

Experiment 1

Hypothesis

The experiment aimed to determine whether laser power, scanning speed, and hatch distance significantly affect the surface area of the initial layer of the overhang samples.

Experimental Design

A 2^3 full factorial design with 5 center points was used for this experiment. To identify the low and high values for the experiment's factors, the down skin starting point of each factor was modified within a range of plus or minus 10% of its original range.

Table 1: Parameter settings for the experiment

Factors	Low	Center Point	High
Laser Power (W)	85.5	95	104.5
Scanning Speed (mm/s)	706.5	785	863.5
Hatch Distance (mm)	0.09	0.1	0.11

Experimental Setup

The experiment was performed using an EOS M 290 machine as shown in figure 5. This machine has a build volume of 250 x 250 x 325 mm. The machine operates using a 1 x 400W Yb-fiber laser with 1 F-theta-lens High-speed scanner, which enables it to scan at an incredibly fast speed of up to 7.0m/s. The laser's focus diameter is approximately 100µm (0.0039 in), which ensures precision and accuracy in the experiment's results. The machine is powered by a 1 x 32A power supply and maximum power consumption of 8.5KW of power (typically 2.4KW). The compressed air supply operates at 7 Bar, with 20 cubic meters per hour, which helps to maintain a stable and controlled environment for the experiment (*EOS M 290*, n.d.).

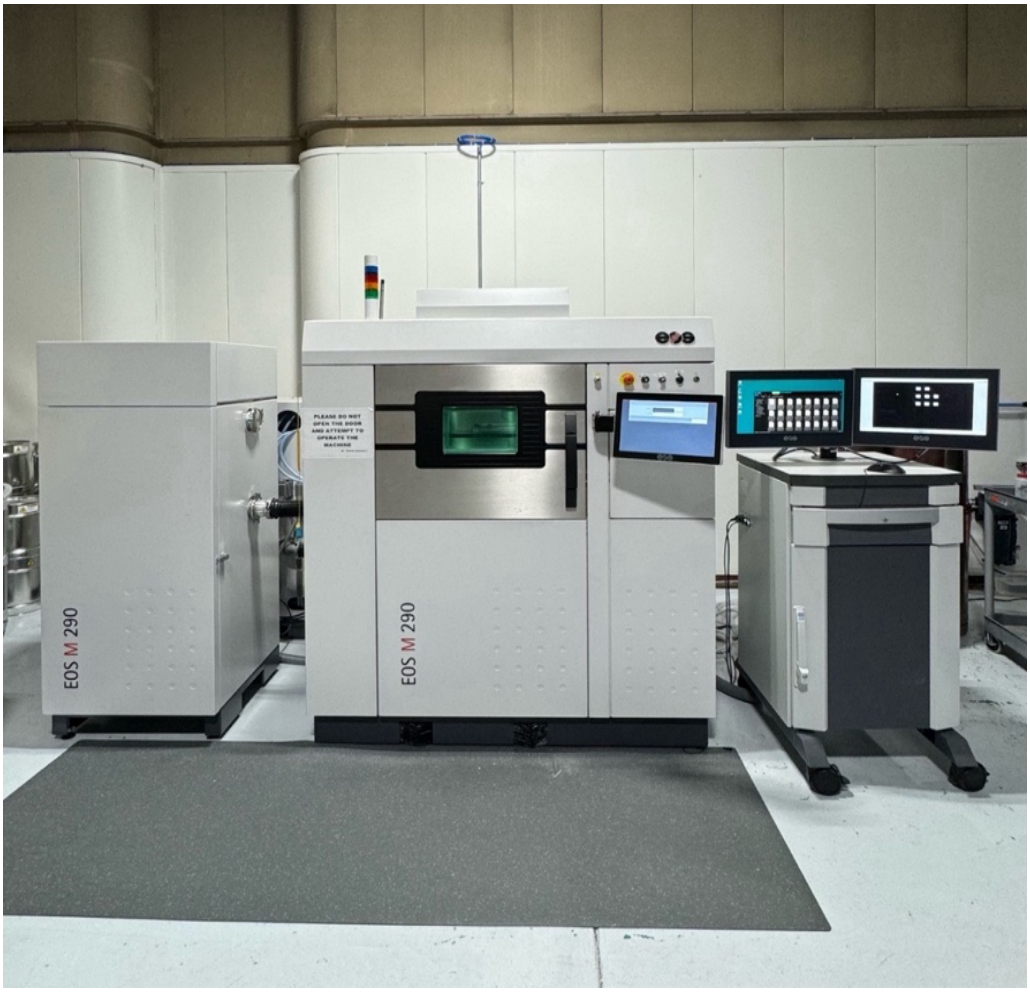

Figure 5 : EOS M 290

Materials

Commercially purchased Inconel 718 powder was used to print samples and the composition of the powder is provided in table 2.

Table 2: Composition of Inconel 718 powder

Element	Ni	Cr	Fe	Nb	Mo
wt%	52.61	17.15	Balance	4.94	2.90
Element	Ti	Al	Mn	Si	Co
wt%	0.89	0.52	0.03	<0.02	0.068
Element	Cu	C	Ta	P	S
wt% / ppm	0.037	0.027	0.006	22	<15
Element	B	Se	Pb	Bi	H
ppm	29	<1	2	0.3	2
Element	Ag	N	O		
ppm	<1	50	110		

Method

To print overhang samples, 10 x 10 x 2 mm supports were generated. The support and 10 x 10 x 10 mm sections were printed using default parameter settings, while the 12 x 10 x 0.12mm overhang sections were printed using the factorial design.

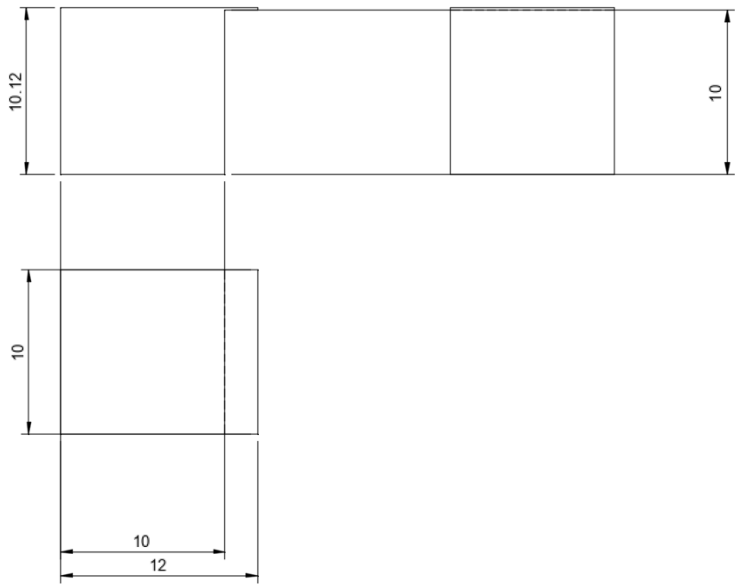

Figure 6: 2D Drawing of overhang sample

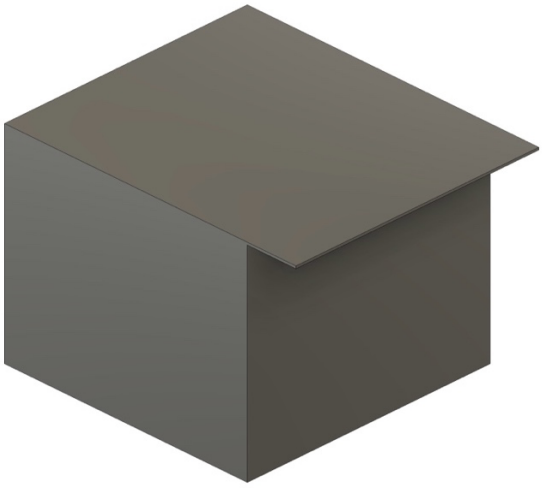

Figure 7: 3D Model of overhang sample

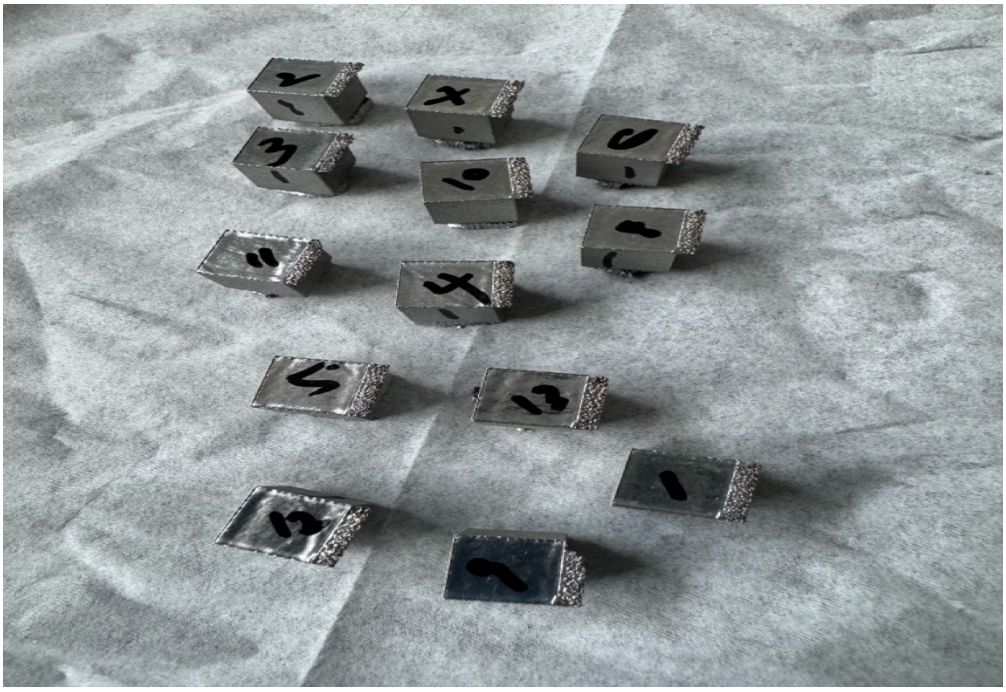

Figure 8: Selective laser melted overhang samples

Surface Area Measurement

The Keyence VHX 7000 Digital Microscope was used to measure the surface area of the overhang samples. This high-resolution microscope produces images similar to those produced by an SEM. The VHX 7000 Microscope has an optical shadow effect mode equipped with specialized high-resolution lenses, a 4K CMOS, and high-performance lighting, which allows for detailed observation and analysis of tiny surface details. The motorized turret also enables easy magnification transitions from 20x to 6000x (Keyence VHX 7000 Series Digital Microscope, n.d.).

To measure the surface area of the overhang samples, the VHX E100 lens was set to a resolution of 80x. This lens resolution allowed for high-quality images of the samples, which were then cropped using the image stitch tool. The measurement function was used to determine the surface area by selecting the area and specifying its rectangular shape. To extract the surface area point cloud data as a CSV file, the surface brightness was specified and the Blck measurement function was selected. The resulting CSV file contained the surface area measurement.

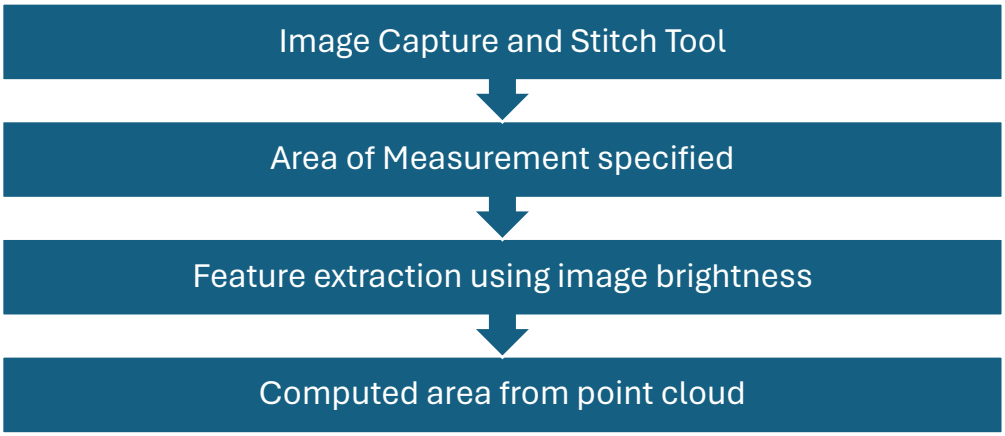

Figure 9: Flow diagram of surface area measurement process.

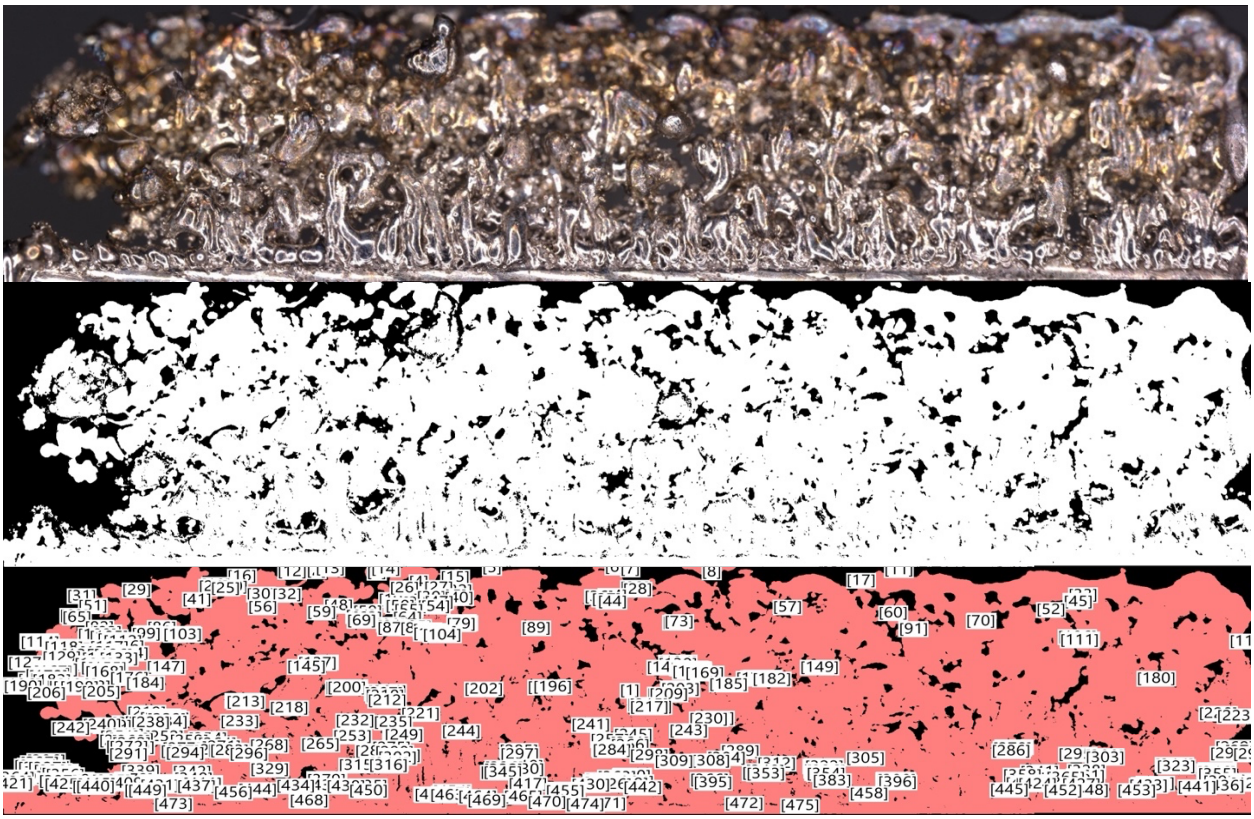

Figure 10: Overhang image, area specified by brightness and point cloud images

Figure 11: Keyence VHX 7000 Series Digital Microscope used for surface area measurement

Analysis

The significance of each process parameter on the surface area was explored by performing an analysis of variance using R. Table 3 shows the results from the ANOVA.

Table 3: Results from ANOVA

	DF	Sum Sq	Mean Sq	F Value	Pr(>F)
Laser Power	1	3.01	3.01	0.560	0.4880
Scanning Speed	1	9.88	9.88	1.835	0.2335
Hatch Distance	1	43.01	43.01	7.992	0.0368
Laser Power: Scanning Speed	1	0.30	0.30	0.056	0.8226
Laser Power :Hatch Distance	1	0.75	0.75	0.139	0.7242
Scanning Speed : Hatch Distance	1	11.16	11.16	2.074	0.2094
Laser Power : Scanning Speed : Hatch Distance	1	0.27	0.27	0.050	0.8316
Residuals	5	26.91	5.38		

The significant level used for this analysis was $\alpha = 0.05$. Factors with a Pr(>F) less than 0.05 are statistically significant whereas factors with Pr(>F) greater than 0.05 are statistically insignificant. From Table 3, only the hatch distance has an effect on surface area. The main effect plot in Figure 12 shows that reducing the hatch distance increase the surface area

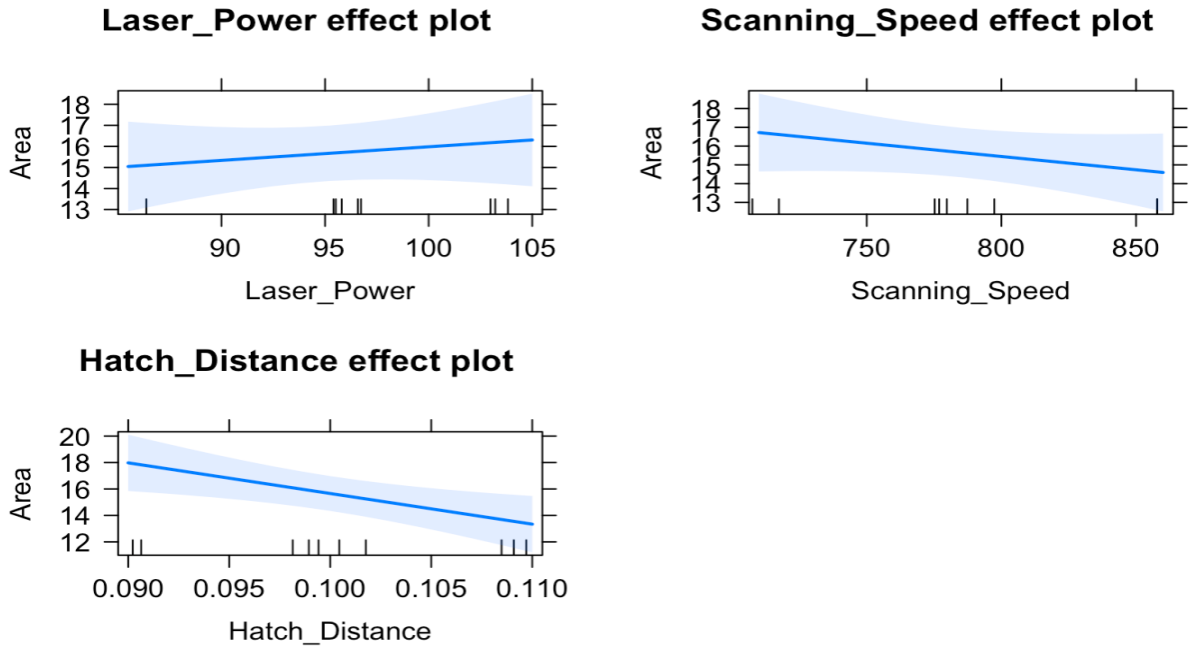

Figure 12: Main Effect Plot

Figure 13 – 25 shows the surface area from the experiment.

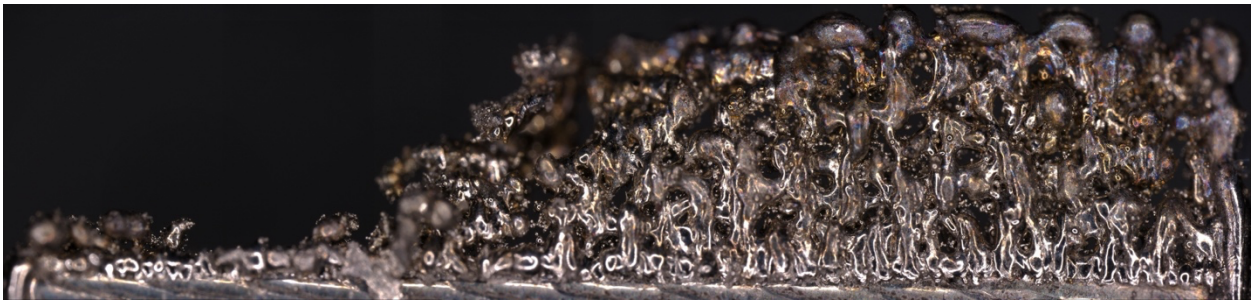

Figure 13: Run 1

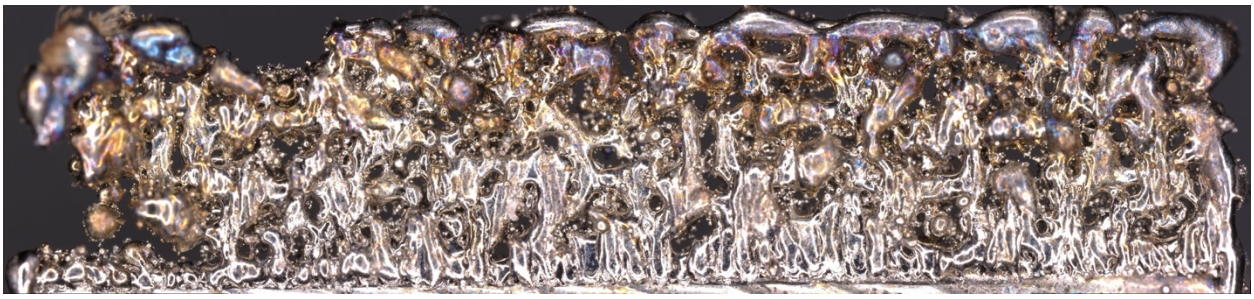

Figure 14:Run 2

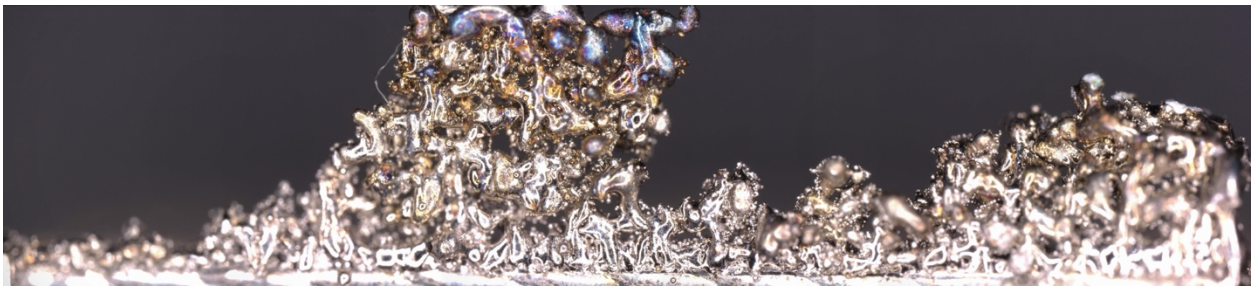

Figure 15: Run 3

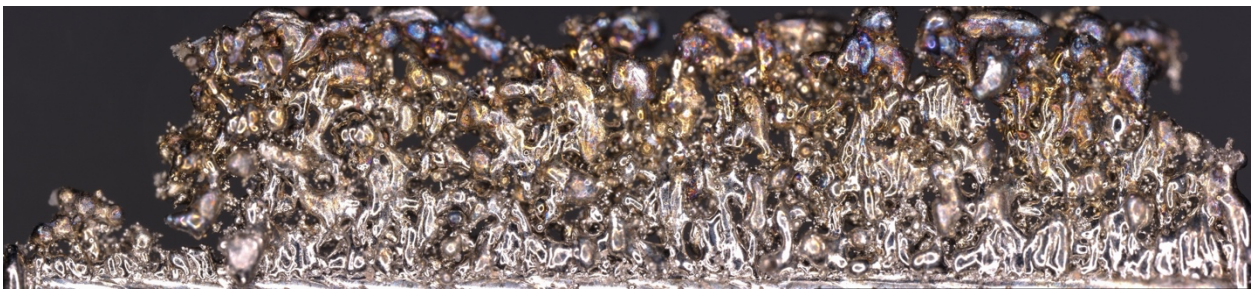

Figure 16: Run 4

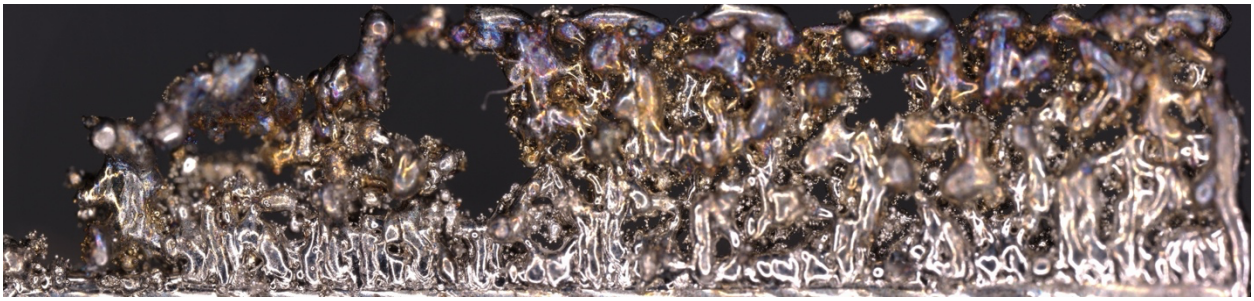

Figure 17: Run 5

Figure 18: Run 6

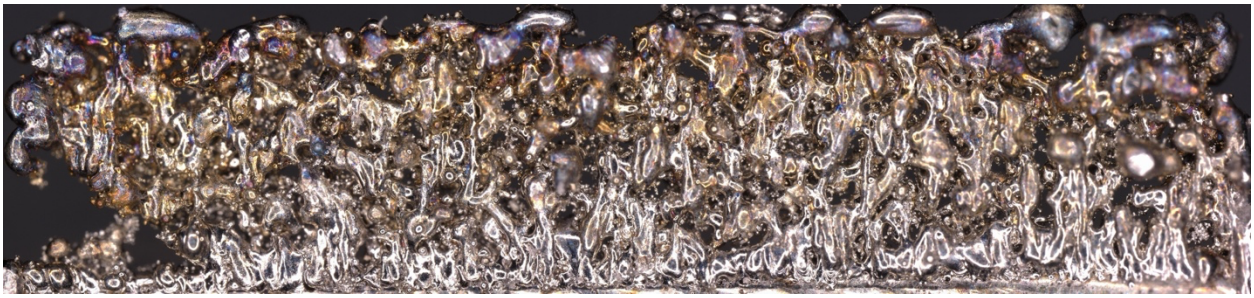

Figure 19: Run 7

Figure 20: Run 8

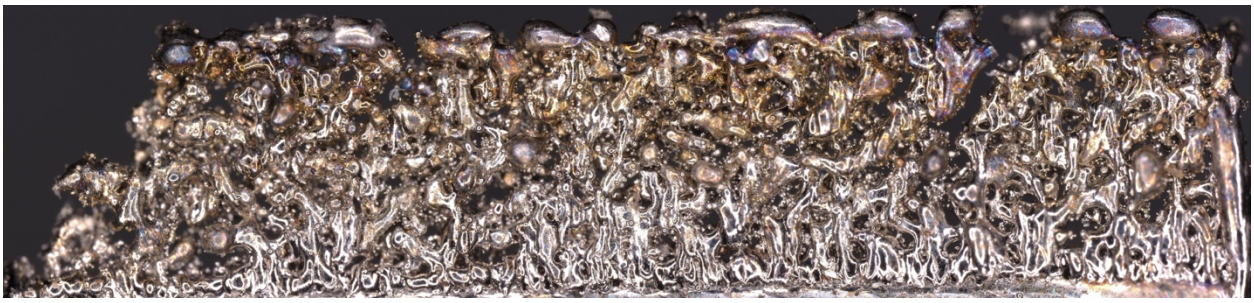

Figure 21: Run 9

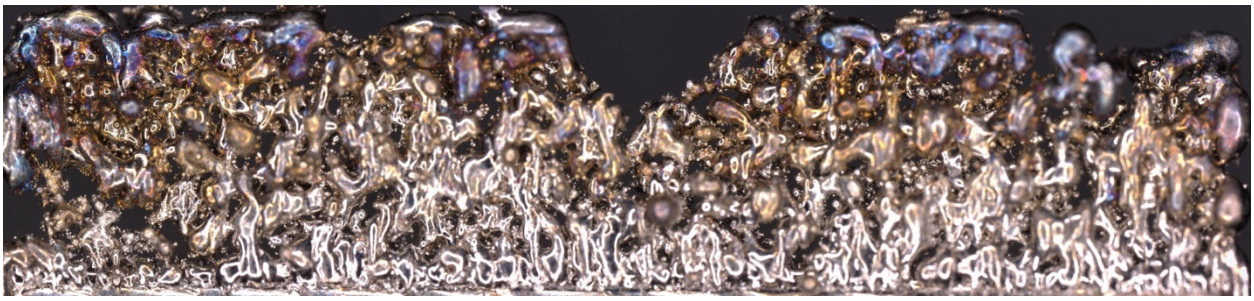

Figure 22: Run 10

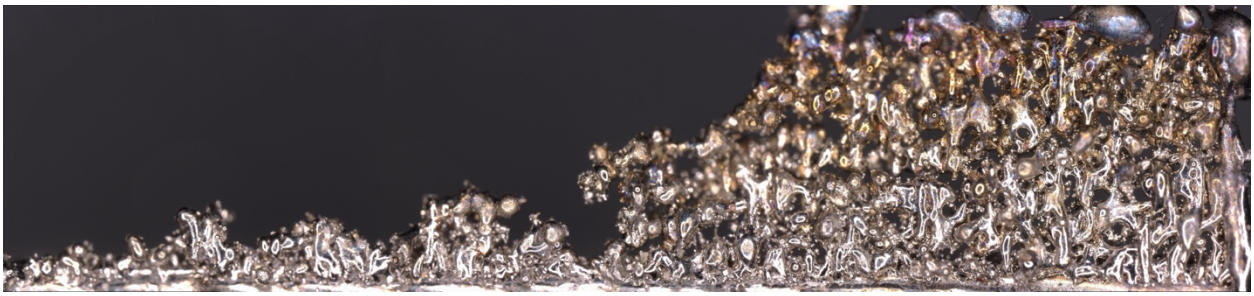

Figure 23: Run 11

Figure 24: Run 12

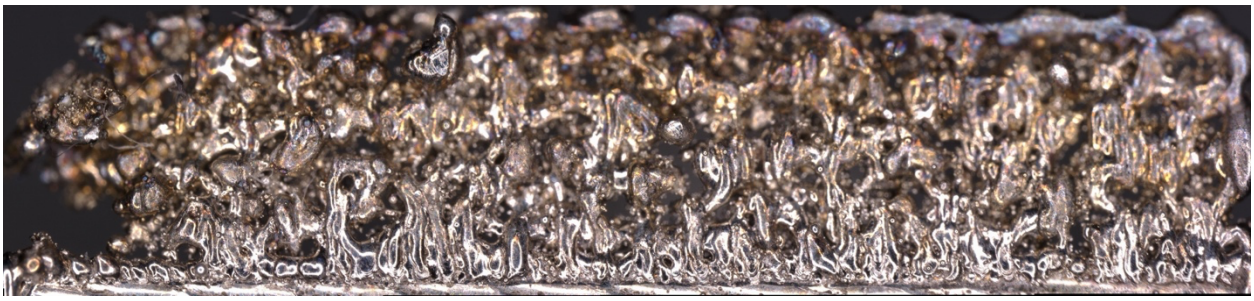

Figure 25: Run 13

Step 2 Experiment

Given the conclusion from the ANOVA, the hatch distance was decreased from the center point using a fixed delta ($\delta = 0.002$). The hatch distance was decreased until the surface area stopped increasing.

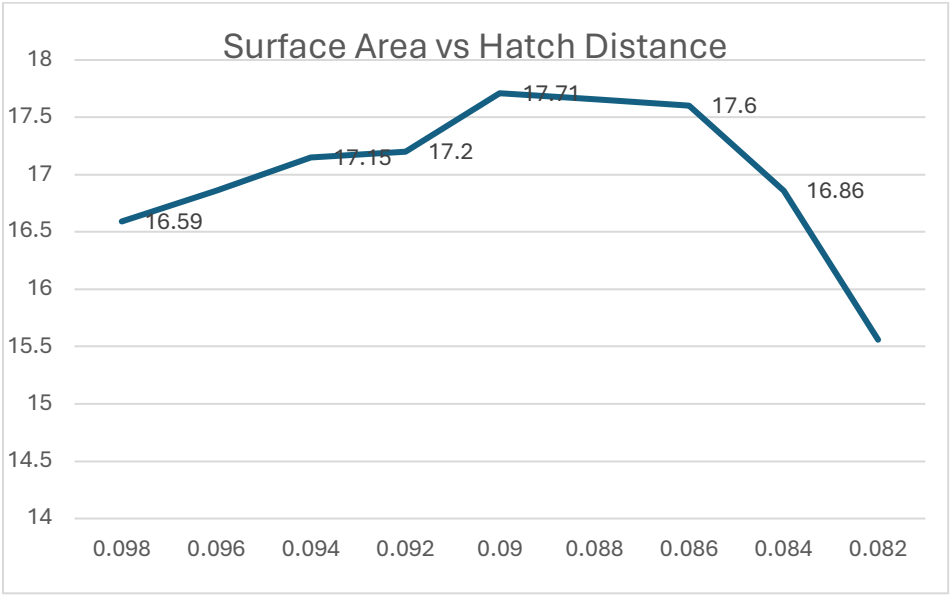

Figure 26: Line plot of Surface Area vs Hatch Distance

The line plot in Figure 26 shows the relationship between the hatch distance and Surface Area. The Surface area increased until 0.09mm hatch distance. Figures 27 to 35 show the overhang images at various hatch distances.

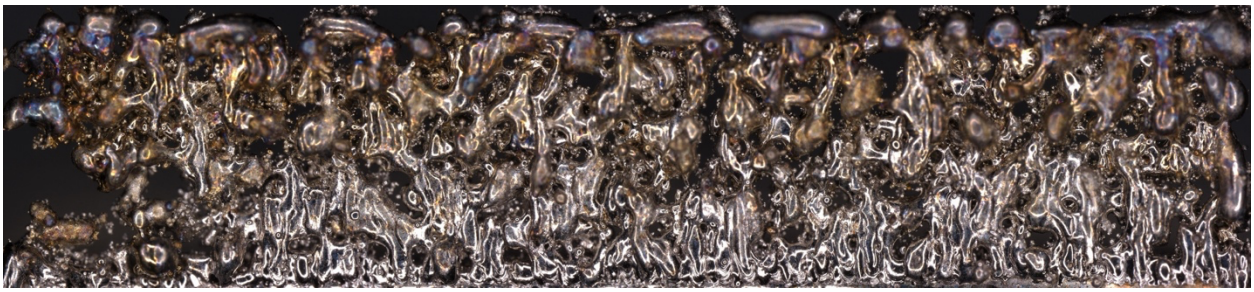

Figure 27: Hatch Distance – 0.098mm

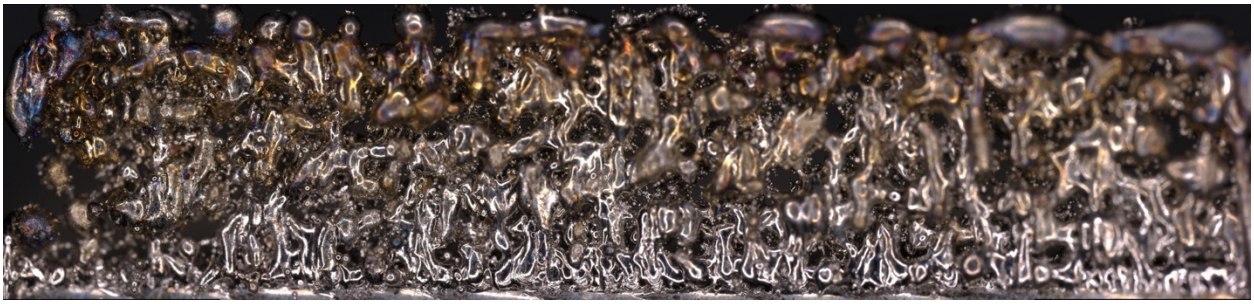

Figure 28: Hatch Distance – 0.096mm

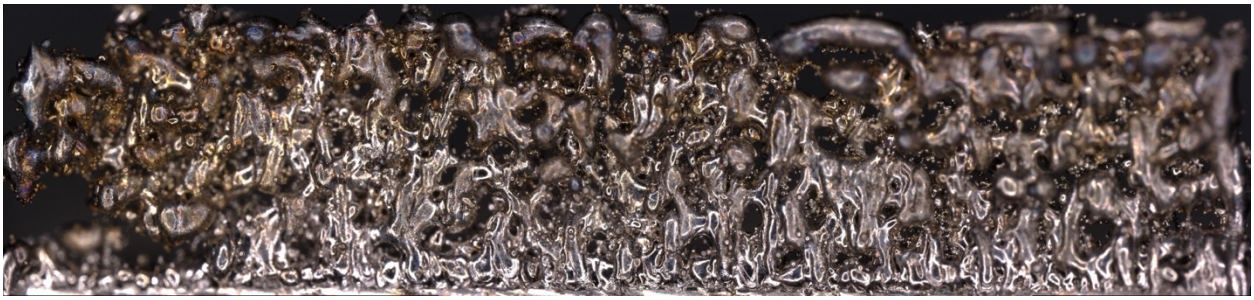

Figure 29: Hatch Distance – 0.094mm

Figure 30: Hatch Distance – 0.092mm

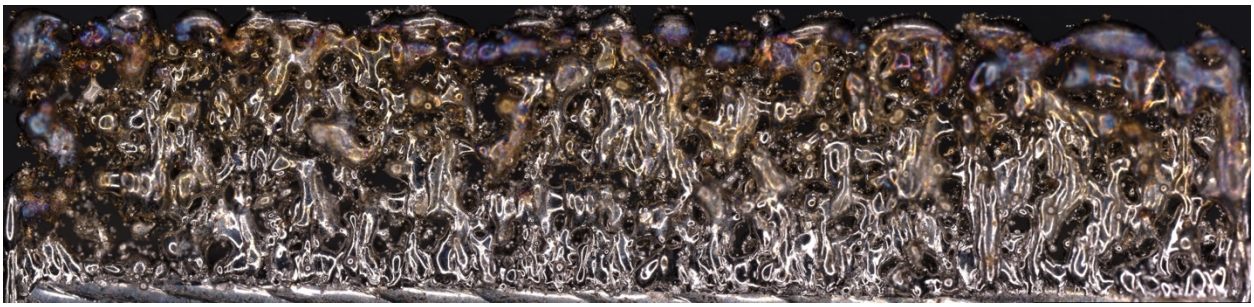

Figure 31: Hatch Distance – 0.090mm

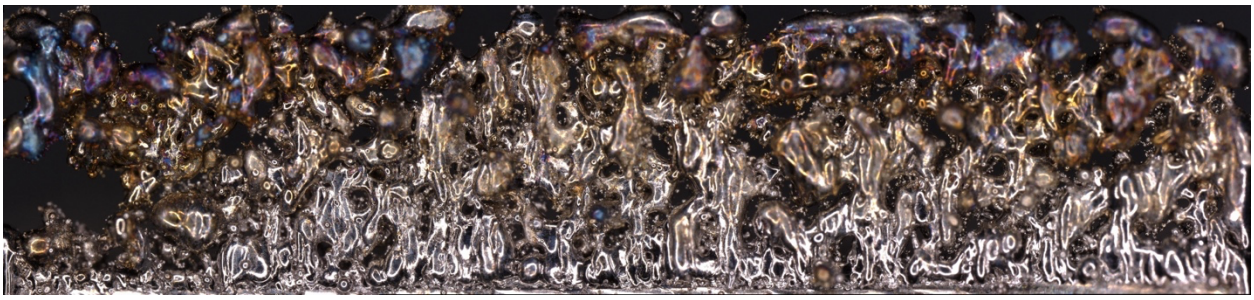

Figure 32: Hatch Distance – 0.088mm

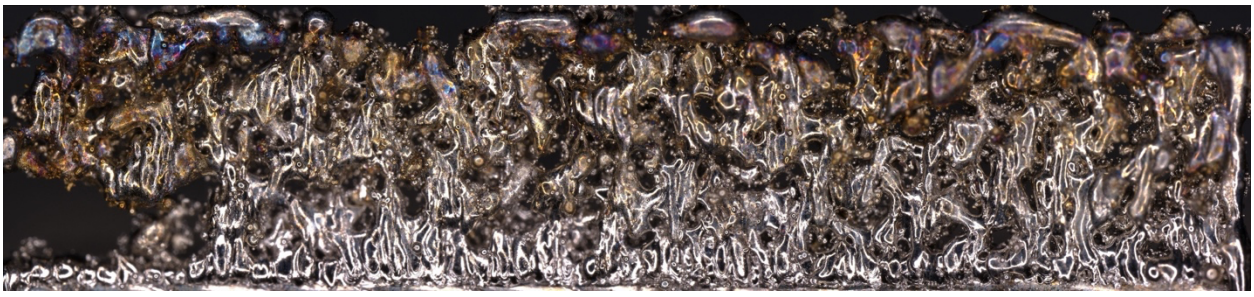

Figure 33: Hatch Distance – 0.086mm

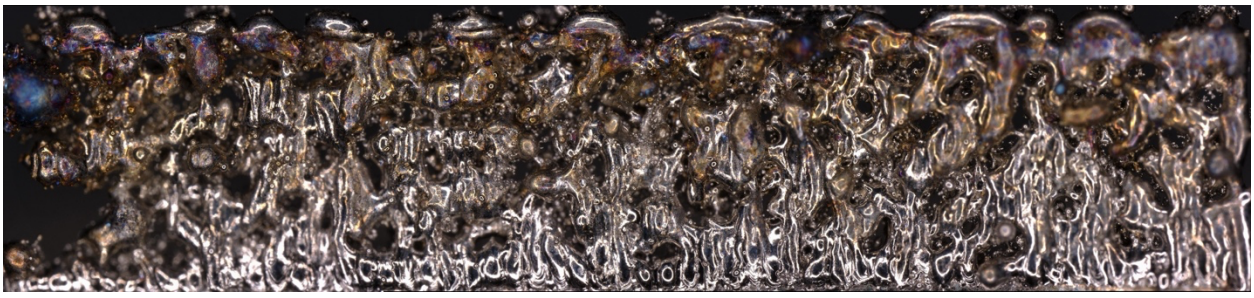

Figure 34: Hatch Distance – 0.084mm

Figure 35: Hatch Distance – 0.082mm

Central Composite Design

A central composite design with 3 factors, 8 factorial points,6 center points, and 6 axial points was used for this experiment. The new center points were used in this experiment. To identify the low and high values for the experiment's factors, the center point of each factor was modified within a range of plus or minus 10% of its original range and $\alpha = 1.68179$ was used to determine axial points.

Table 4: Parameter settings for response surface experiment

Factors	-α	-1	0	+1	+α
Laser Power (W)	79.0229	85.5	95	104.5	110.9771
Scanning Speed (mm/s)	652.9787	706.5	785	863.5	917.0213
Hatch Distance (mm)	0.074864	0.081	0.09	0.099	0.105136

Analysis

Table 5: ANOVA Results

Source	DF	Adj SS	Adj MS	F-Value	P-Value
Model	9	46.9506	5.2167	2.24	0.112
Linear	3	28.9693	9.6564	4.15	0.038
Laser Power	1	8.4248	8.4248	3.62	0.086
Scanning Speed	1	12.7354	12.7354	5.48	0.041
Hatch Distance	1	7.8091	7.8091	3.36	0.097
Square	3	7.3915	2.4638	1.06	0.409
Laser Power*Laser Power	1	7.0208	7.0208	3.02	0.113
Scanning Speed*Scanning Speed	1	0.1138	0.1138	0.05	0.829
Hatch Distance*Hatch Distance	1	0.0838	0.0838	0.04	0.853
2-Way Interaction	3	10.5898	3.5299	1.52	0.269
Laser Power*Scanning Speed	1	0.6659	0.6659	0.29	0.604
Laser Power*Hatch Distance	1	1.7187	1.7187	0.74	0.410
Scanning Speed*Hatch Distance	1	8.2053	8.2053	3.53	0.090
Error	10	23.2556	2.3256		
Lack-of-Fit	5	13.0793	2.6159	1.29	0.395
Pure Error	5	10.1763	2.0353		
Total	19	70.2063			

Based on the ANOVA result in Table 5, it was found that Scanning speed was significant at alpha level of 0.05 as shown in Figure 36. At alpha level of 0.10, Scanning speed, Laser power, Hatch distance, and the interaction between Scanning Speed and Hatch Distance were significant as shown in Figure 37. Figure 38 shows that at alpha level of 0.15, Scanning speed, Laser power, Hatch distance, the interaction between Scanning Speed and Hatch Distance, and Laser Power were all found to be significant.

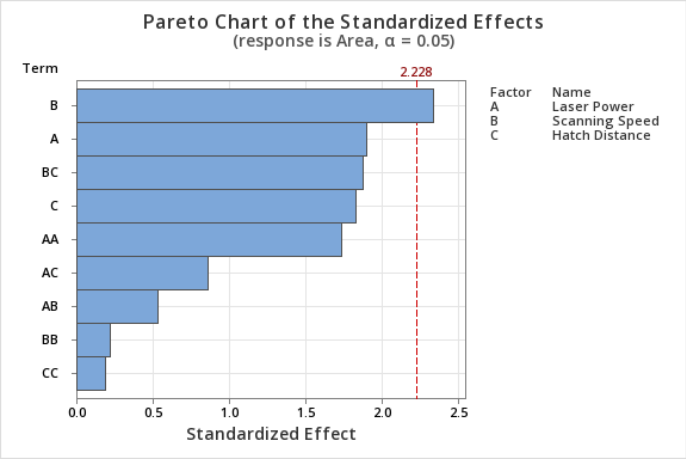

Figure 36: Pareto Chart of the standardized effects at α=0.05

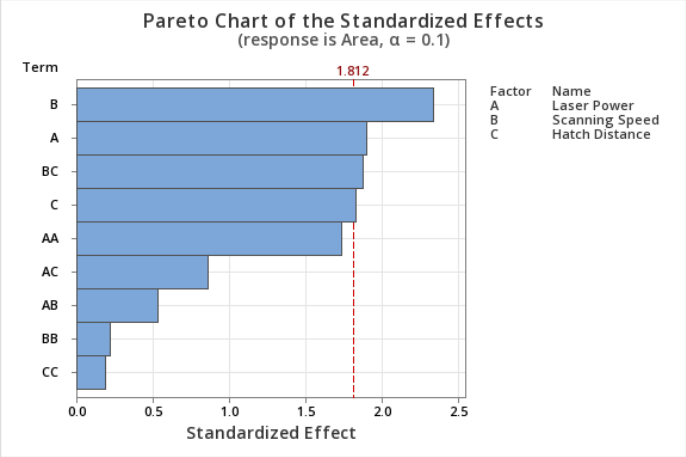

Figure 37: Pareto Chart of the standardized effects at α=0.1

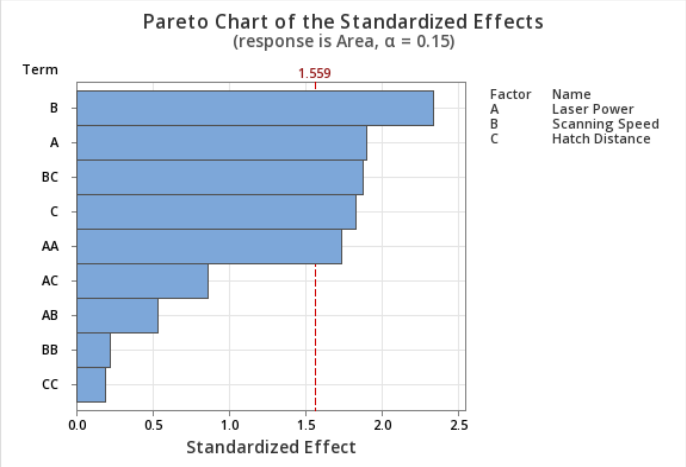

Figure 38: Pareto Chart of the standardized effects at α=0.15

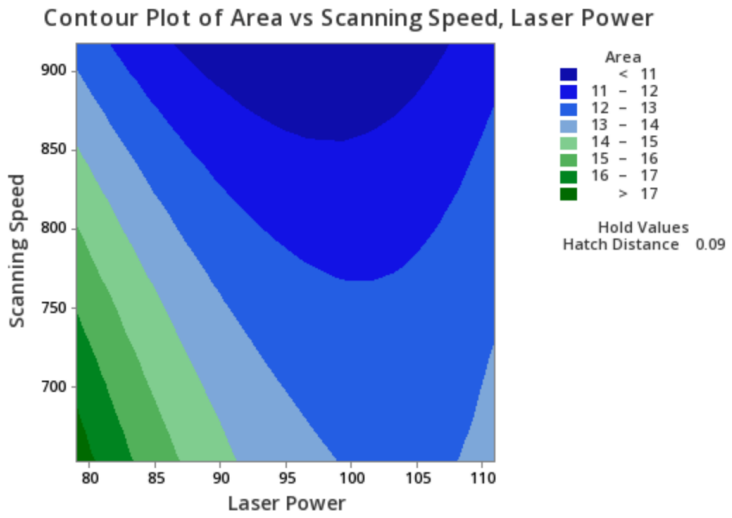

Figure 39: Contour plots of Area vs Scanning Speed, Laser Power

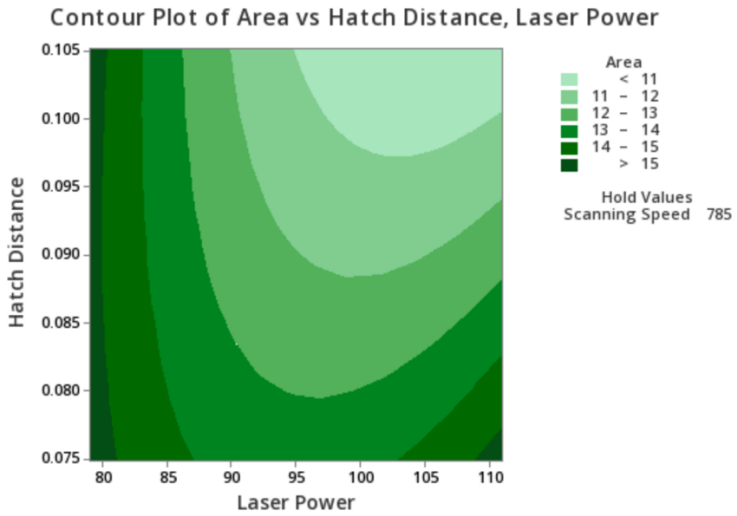

Figure 40: Contour plot of Area vs Hatch Distance Laser Power

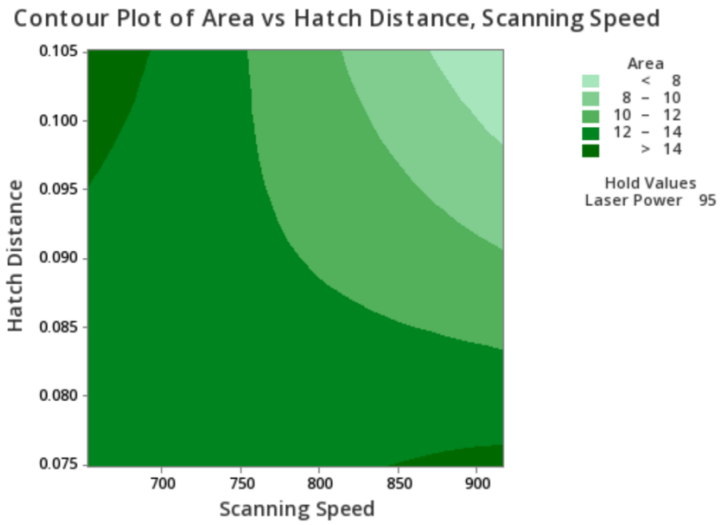

Figure 41: Contour plot of Area vs Hatch Distance, Scanning Speed

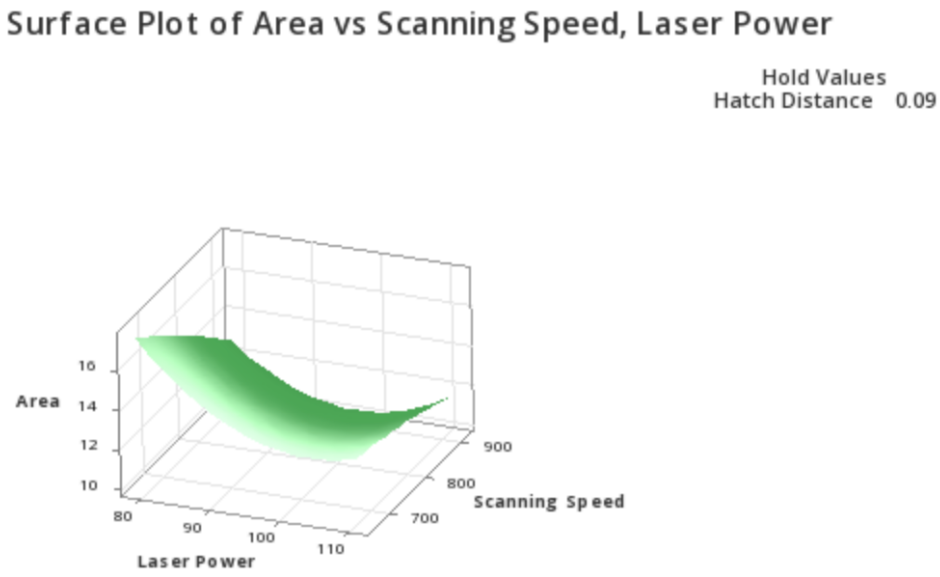

Figure 42: Surface plot of Area vs Scanning Speed, Laser Power

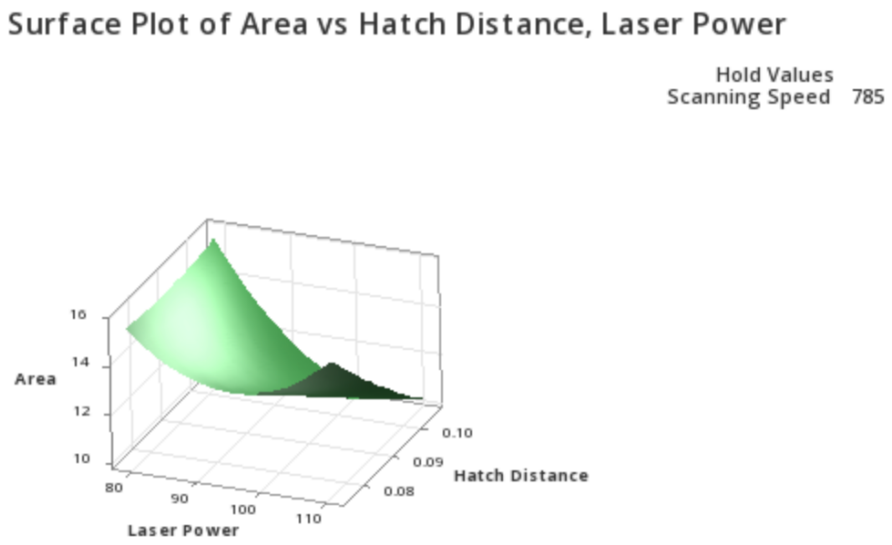

Figure 43: Surface Plot of Area vs Hatch Distance, Laser Power

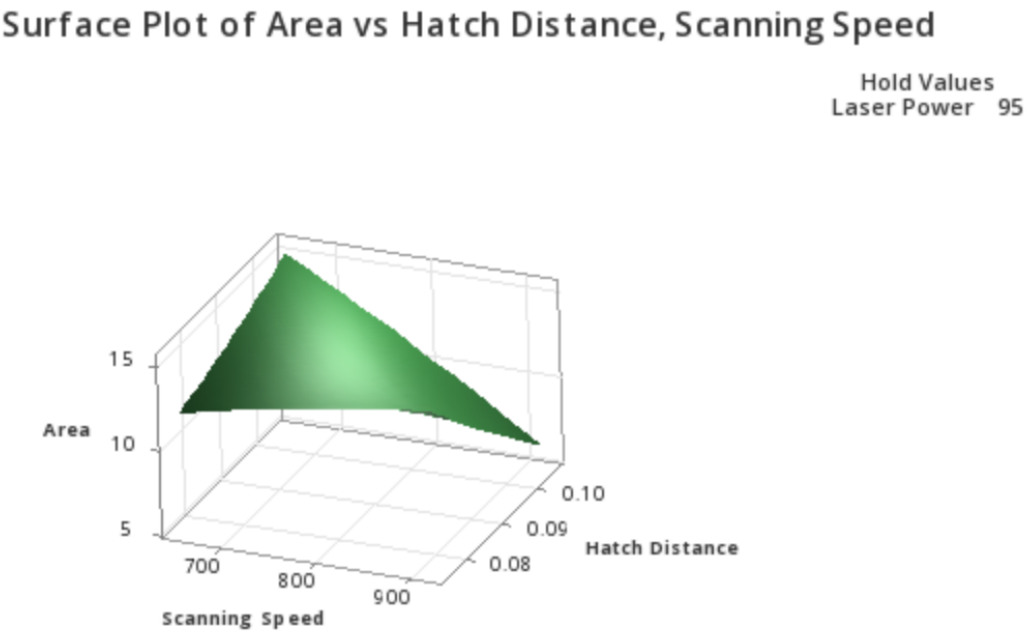

Figure 44: Surface Plot of Area vs Hatch Distance, Scanning Speed

The contour plot in Figure 39 shows that a surface area greater than 17mm^2 can be achieved around a laser power of 80W, scanning speed of 670mm/s, and hatch distance of 0.09mm. Figure 40 shows that a surface area greater than 15mm^2 can be achieved around the region of laser power of 80W and 110W respectively, scanning speed of 785mm/s, and hatch distance between 0.075mm – 0.105mm. The contour plot in Figure 41 shows a surface area greater than 14mm^2 can be achieved around the region of laser power of 95W, scanning speed between 850mm/s - 920mm/s, and a hatch distance of 0.075mm.

Response optimizer in Minitab was used to optimize the surface area by setting the target value to 20mm^2. The result as shown in Figure 45 indicates that this target value can be achieved by setting Laser power to 79.0230W, scanning speed 652.9793mm/s, and hatch distance 0.1022mm.

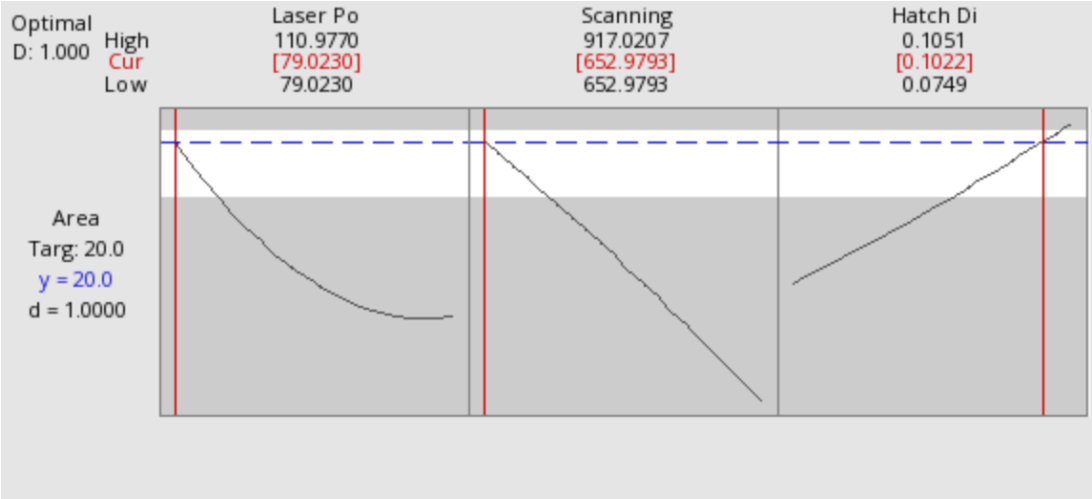

Figure 45: Optimized SLM process parameters from Minitab.

Sample Images

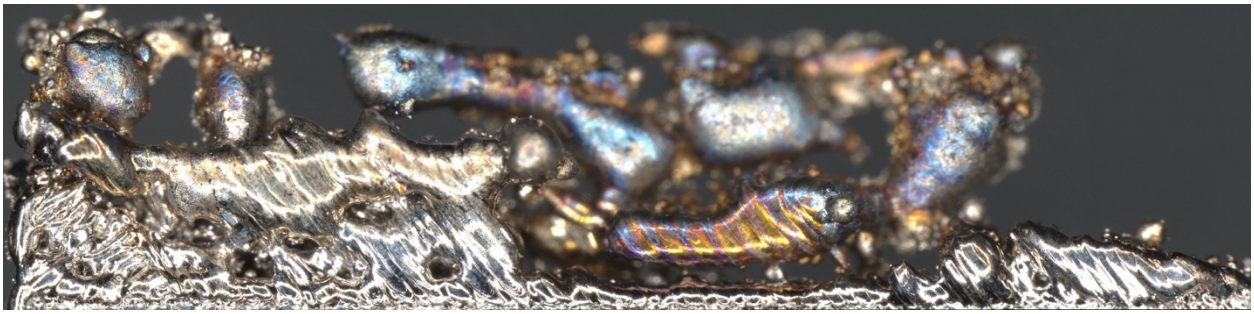

Figure 46: Run 1

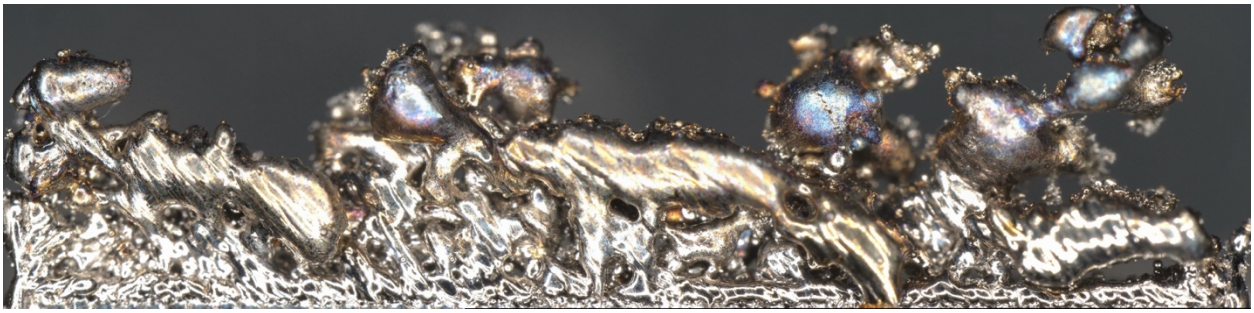

Figure 47: Run 2

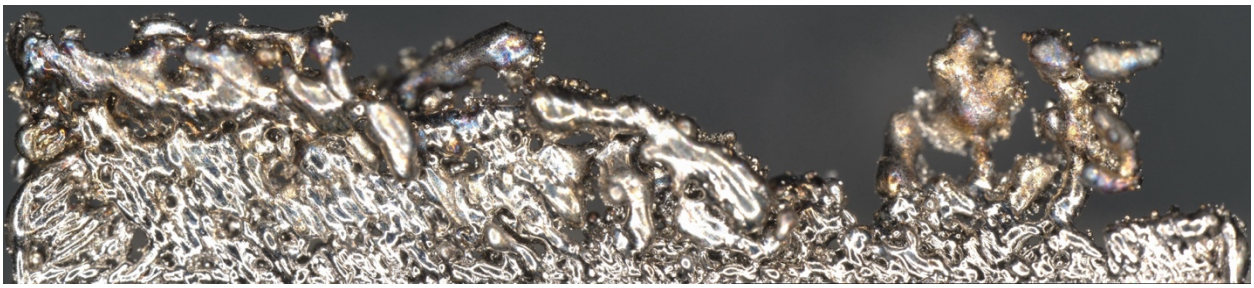

Figure 48: Run 3

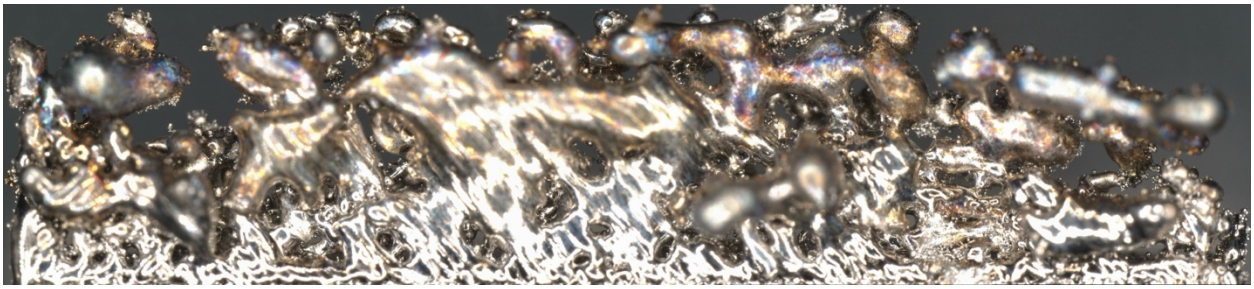

Figure 49: Run 4

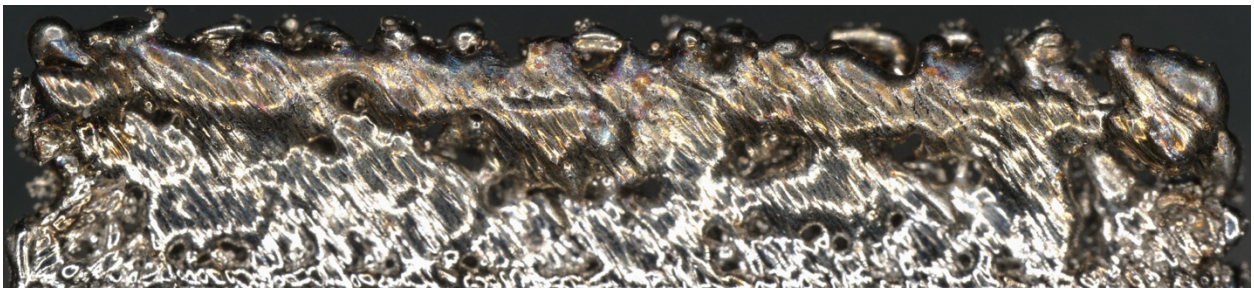
Figure 50: Run 5

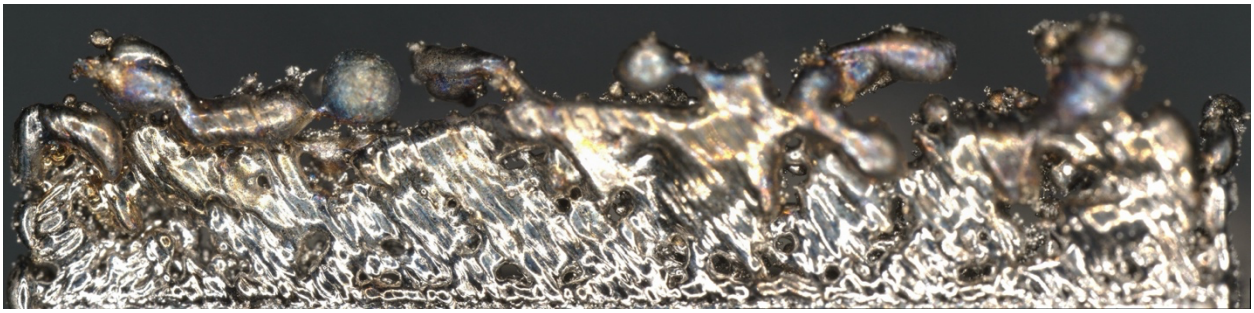
Figure 51: Run 6

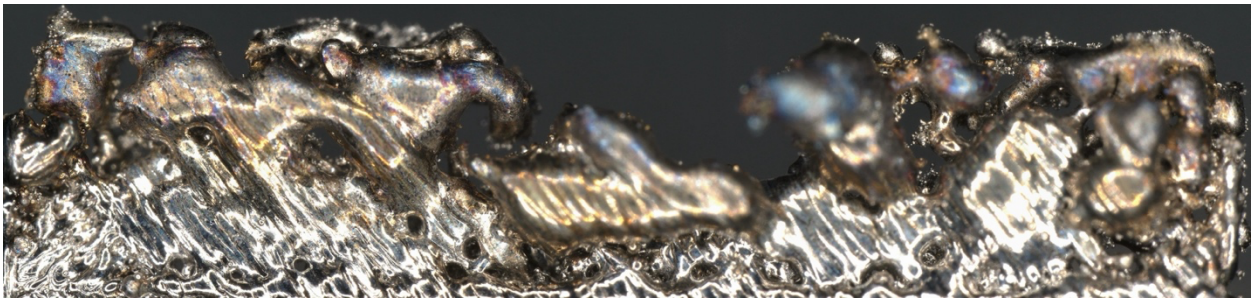
Figure 52: Run 7

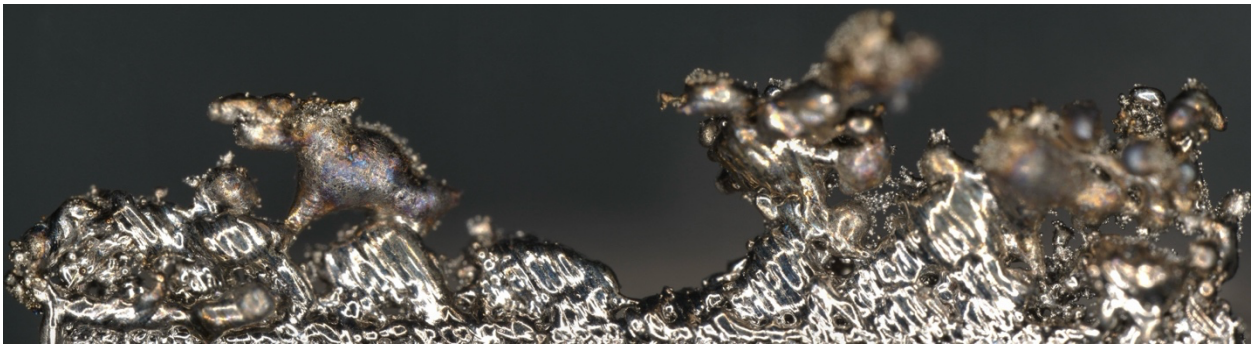
Figure 53: Run 8

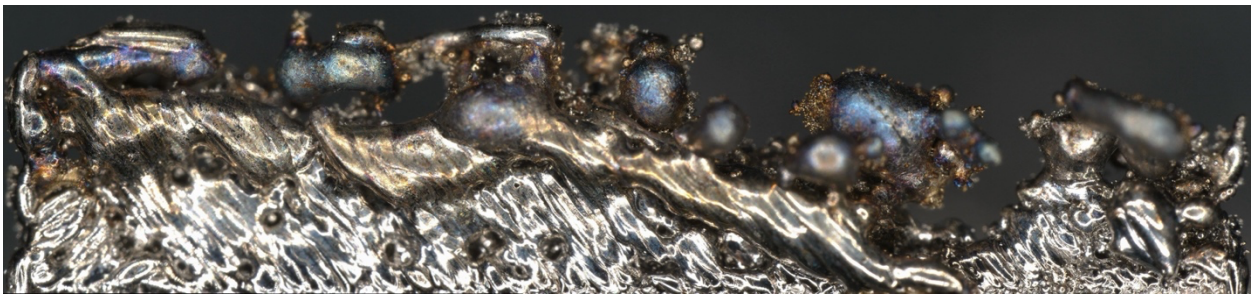

Figure 54: Run 9

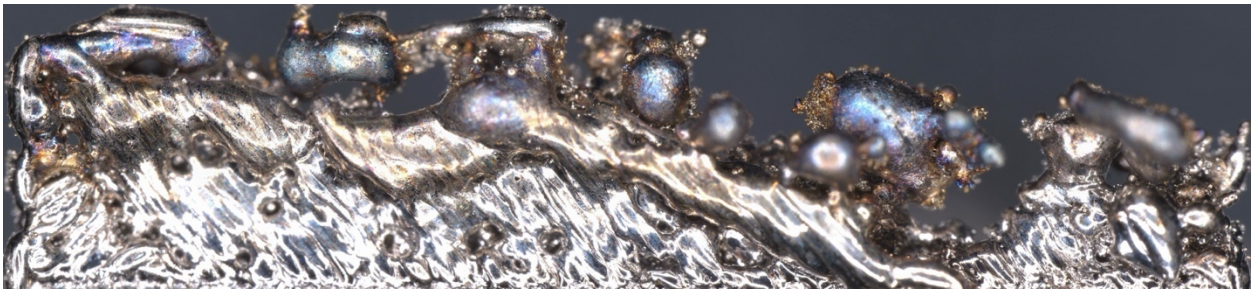

Figure 55: Run 10

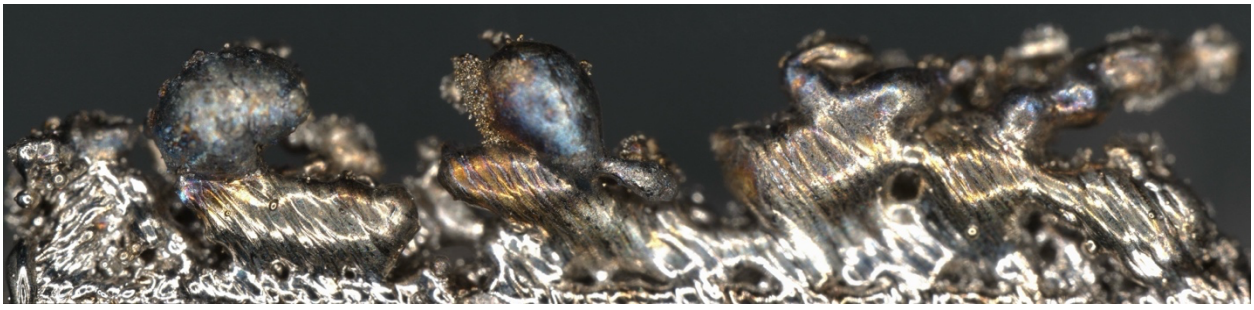

Figure 56: Run 11

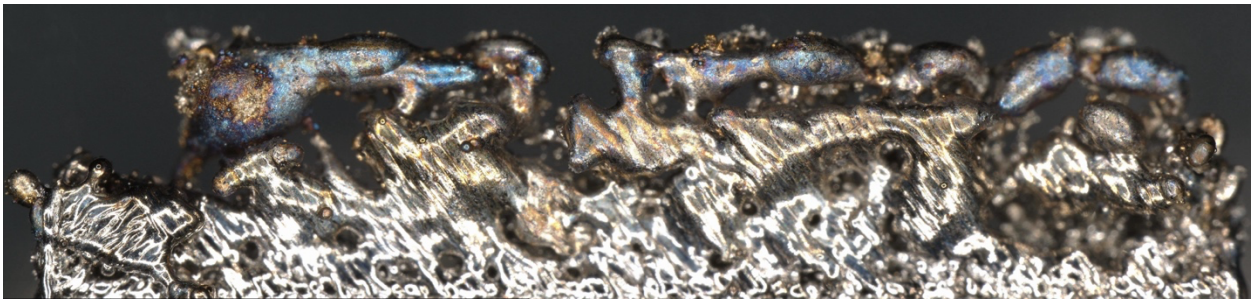

Figure 57: Run 12

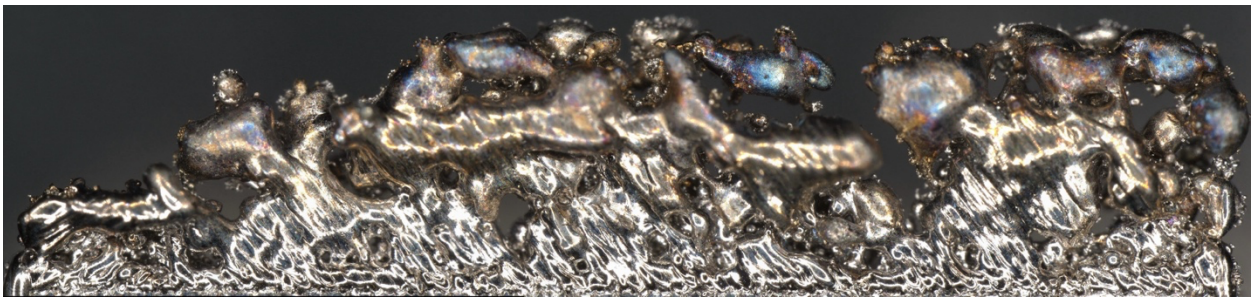

Figure 58: Run 13

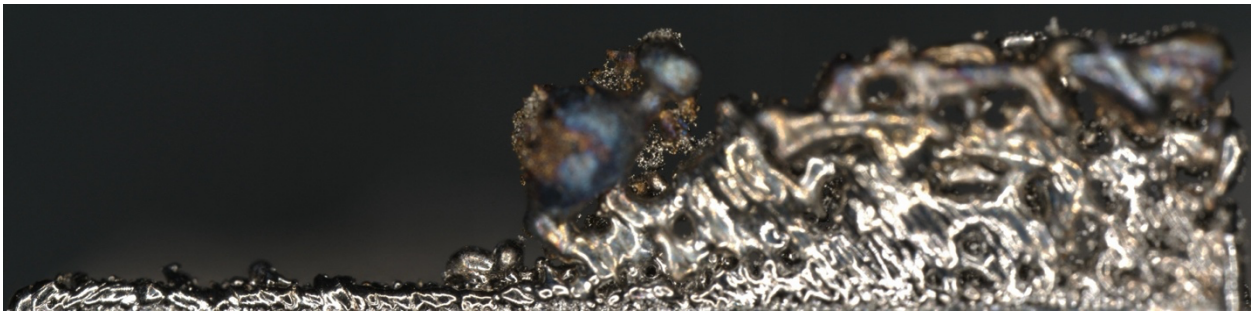

Figure 59: Run 14

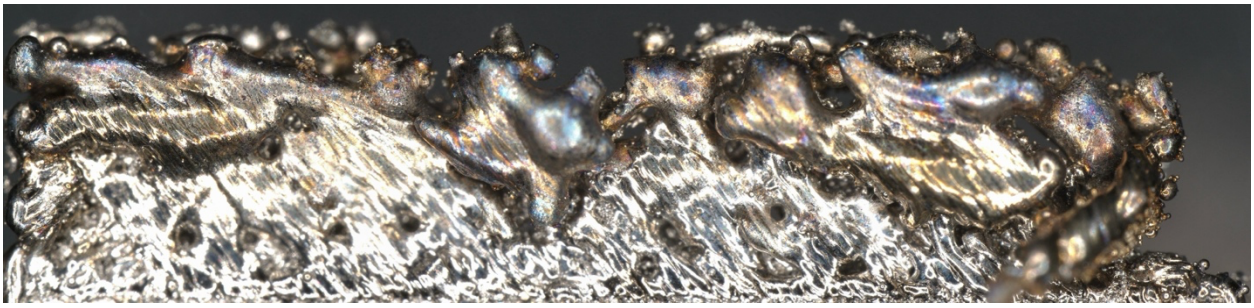

Figure 60: Run 15

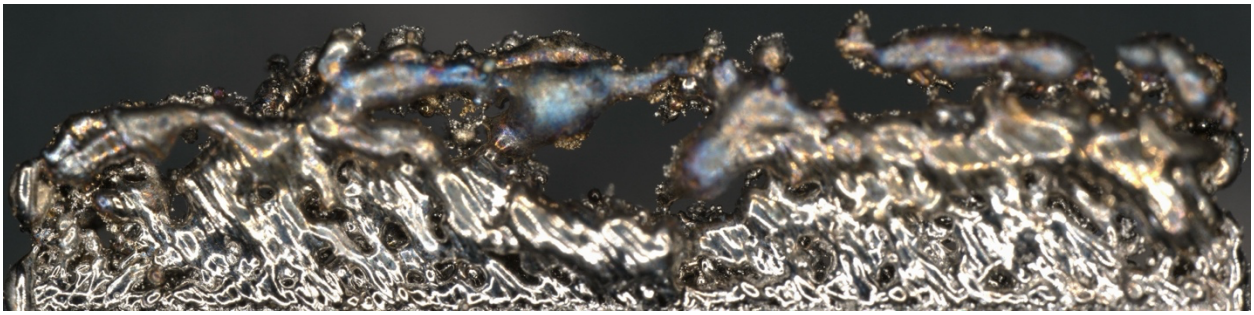

Figure 61: Run 16

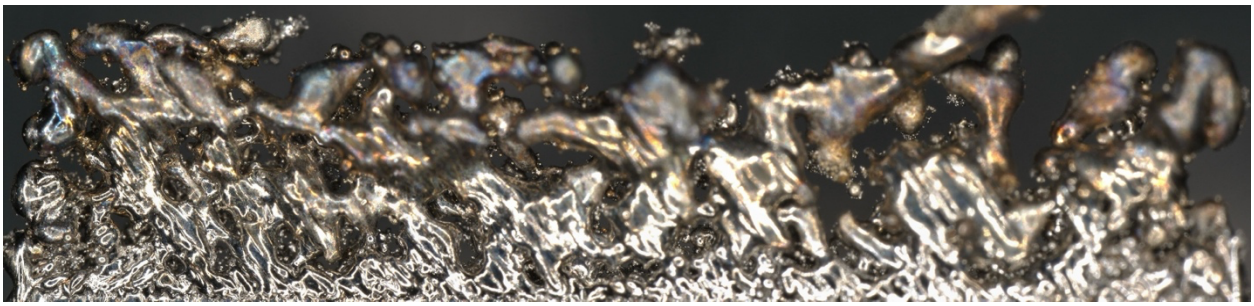
Figure 62: Run 17

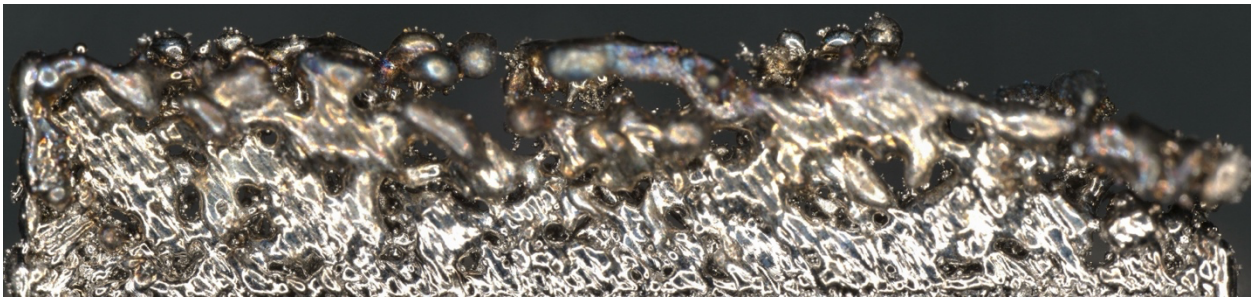
Figure 63: Run 18

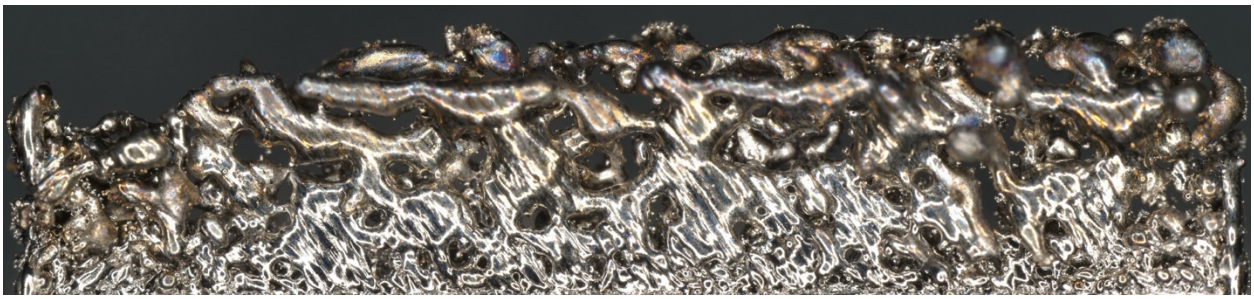
Figure 64: Run 19

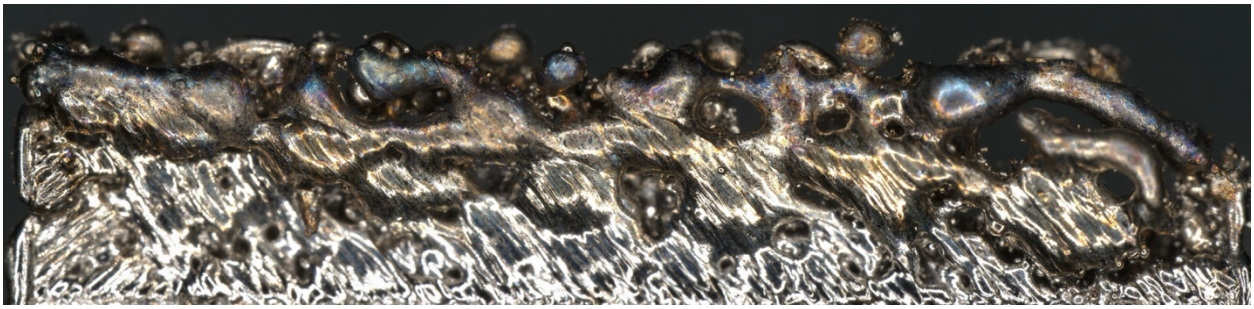
Figure 65: Run 20

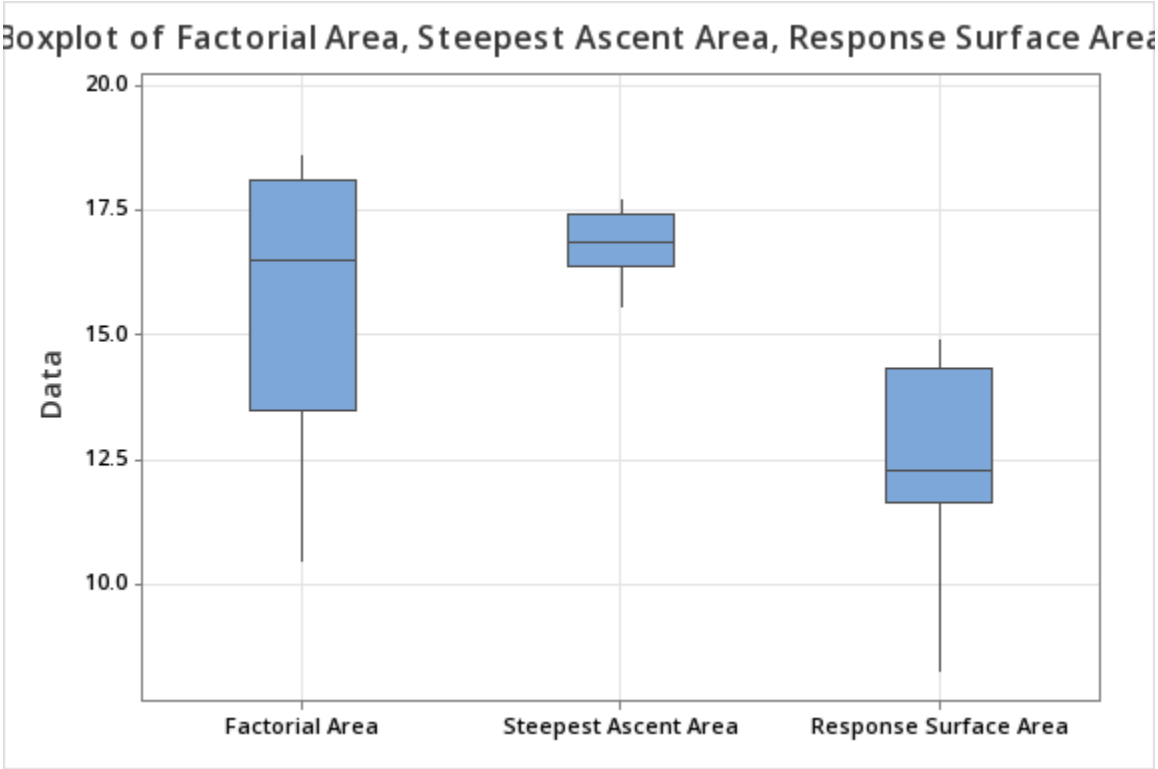

Figure 66: Boxplot of Factorial Area, Steepest Ascent Search Area and Response Surface Area

CHAPTER IV

CONCLUSION

RSM was used to identify SLM parameter settings that optimize the surface area of the initial layer of supportless horizontal overhang structure. This was done in 3 -step experiments. For experiment 1, a 2^3 full factorial design with 5 center points was used in this experiment. The surface area of the samples was measured using VHX 7000 Series Digital Microscope. The ANOVA results from this experiment at $\alpha = 0.05$ indicated that hatch distance was the only significant factor and reducing the hatch distance increases the surface area. Based on this result, a second experiment was performed to explore the gradient ascent.

In the second experiment, the hatch distance was reduced by a fixed delta of 0.002. The surface area continued to increase until reaching a hatch distance of 0.090mm. From this experiment, new center points were obtained for the central composite design.

A central composite design with 3 factors, 8 factorial points, 6 center points, and 6 axial points was used in the third experiment. The results from this experiment show that a surface area greater than 17mm^2 can be achieved at laser power of 80W, scanning speed of 670mm/s, and hatch distance of 0.09mm. The results from the response optimizer also indicated a surface area of 20mm^2 can be achieved with Laser power to 79.0230W, scanning speed 652.9793mm/s, and hatch distance 0.1022mm.

A Boxplot plot in figure 66 was used to compare the surface area from each experiment. The second experiment recorded the highest mean surface area while the last experiment recorded the least mean value. It is important to note the EOS M290 machine used for the experiment had major maintenance between the second and third experiments. This leaves the results of this study inconclusive.

For future work, the third experiment will be performed again to validate the results from this experiment. Further study should be conducted to explore the region of surface area increase from the response surface methodology. Experiments should be conducted to optimize process parameters for printing the transition layers of horizontal supportless overhang structures. A complete overhang should be printed with this parameter settings and mechanical properties should be investigated.

REFERENCES

Atzeni, E., & Salmi, A. (2015). Study on unsupported overhangs of AlSi10Mg parts processed by Direct Metal Laser Sintering (DMLS). *Journal of Manufacturing Processes*, *20*, 500 506.

Canacoo, S. K. (2022). *A Study of the Surface Properties of Additive Manufactured Inconel 718 After Laser Surface Treatment and CNC Grinding*.

Carter, L. N., Martin, C., Withers, P. J., & Attallah, M. M. (2014). The influence of the laser scan strategy on grain structure and cracking behaviour in SLM powder-bed fabricated nickel superalloy. *Journal of Alloys and Compounds*, *615*, 338–347.

Chen, H., Gu, D., Xiong, J., & Xia, M. (2017). Improving additive manufacturing processability of hard-to-process overhanging structure by selective laser melting. *Journal of Materials Processing Technology*, *250*, 99–108.

Cheng, B., Shrestha, S., & Chou, K. (2016). Stress and deformation evaluations of scanning strategy effect in selective laser melting. *Additive Manufacturing*, *12*, 240–251.

EOS M 290. (n.d.). https://www.eos.info/en-us/metal-solutions/metal-printers/eos-m-290#key-features

Ferrar, B., Mullen, L., Jones, E., Stamp, R., & Sutcliffe, C. (2012). Gas flow effects on selective laser melting (SLM) manufacturing performance. Journal of Materials Processing Technology, 212(2), 355–364.

Fox, J. C., Moylan, S. P., & Lane, B. M. (2016). Effect of process parameters on the surface roughness of overhanging structures in laser powder bed fusion additive manufacturing. Procedia Cirp, 45, 131–134.

Gu, D., Zhang, H., Chen, H., Zhang, H., & Xi, L. (2020). Laser additive manufacturing of high-performance metallic aerospace components. Chinese Journal of Lasers, 47(5), 0500002.

He, L., Zi, F., Zhang, Z., Tang, L., & Li, P. (2019). *Research on the performance of honeycomb support structure based on SLM*. *612*(3), 032148.

Hildreth, O. J., Nassar, A. R., Chasse, K. R., & Simpson, T. W. (2016). Dissolvable metal supports for 3D direct metal printing. *3D Printing and Additive Manufacturing*, *3*(2), 90 97.

Hodge, N., Ferencz, R., & Vignes, R. (2016). Experimental comparison of residual stresses for a thermomechanical model for the simulation of selective laser melting. *Additive Manufacturing*, *12*, 159–168.

Hussein, A., Hao, L., Yan, C., & Everson, R. (2013). Finite element simulation of the temperature and stress fields in single layers built without-support in selective laser melting. *Materials & Design (1980-2015)*, *52*, 638–647. https://doi.org/10.1016/j.matdes.2013.05.070

Hussein, A., Hao, L., Yan, C., Everson, R., & Young, P. (2013). Advanced lattice support structures for metal additive manufacturing. *Journal of Materials Processing Technology*, *213*(7), 1019–1026.

Jiang, J., Chen, J., Ren, Z., Mao, Z., Ma, X., & Zhang, D. Z. (2020). The influence of process parameters and scanning strategy on lower surface quality of TA15 parts fabricated by selective laser melting. *Metals*, *10*(9), 1228.

Keyence VHX 7000 Series Digital Microscope. (n.d.). https://www.keyence.eu/products/microscope/digital-microscope/vhx-7000/

Khairallah, S. A., & Anderson, A. (2014). Mesoscopic simulation model of selective laser melting of stainless steel powder. *Journal of Materials Processing Technology*, *214*(11), 2627–2636.

Kruth, J.-P., Deckers, J., Yasa, E., & Wauthlé, R. (2012). Assessing and comparing influencing factors of residual stresses in selective laser melting using a novel analysis method. *Proceedings of the Institution of Mechanical Engineers, Part B: Journal of Engineering Manufacture*, *226*(6), 980–991.

Lefky, C. S., Zucker, B., Wright, D., Nassar, A. R., Simpson, T. W., & Hildreth, O. J. (2017). Dissolvable supports in powder bed fusion-printed stainless steel. *3D Printing and Additive Manufacturing*, *4*(1), 3–11.

Malians, G., Sarafis, I., Lazaridis, T., Varoutoglou, A., & Tsakataras, G. (2016). *Random lattice structures. Modelling, manufacture and FEA of their mechanical response*. *161*(1), 012045.

Markl, M., & Körner, C. (2016). Multiscale modeling of powder bed–based additive manufacturing. *Annual Review of Materials Research*, *46*, 93–123.

Osakada, K., & Shiomi, M. (2006). Flexible manufacturing of metallic products by selective laser melting of powder. International Journal of Machine Tools and Manufacture, 46(11), 1188–1193.

Shi, W., Wang, P., Liu, Y., & Han, G. (2019). Experiment of process strategy of selective laser melting forming metal nonhorizontal overhanging structure. Metals, 9(4), 385.

Sun, J., Yang, Z., Yang, Y., & Wang, D. (2017). Research on the microstructure and properties of the overhanging structure formed by selective laser melting. *Rapid Prototyping Journal*, *23*(5), 904–910.

Sundar, R., Hedaoo, P., Ranganathan, K., Bindra, K. S., & Oak, S. M. (2014). Application of meshes to extract the fabricated objects in selective laser melting. *Materials and Manufacturing Processes*, *29*(4), 429–433.

Vasileska, E., Demir, A., Colosimo, B., & Previtali, B. (2022). A novel paradigm for feedback control in LPBF: layer-wise correction for overhang structures. *ADVANCES IN MANUFACTURING*, *10*(2), 326–344. https://doi.org/10.1007/s40436-021-00379-6

Wang, D., Mai, S., Xiao, D., & Yang, Y. (2016). Surface quality of the curved overhanging structure manufactured from 316-L stainless steel by SLM. *The International Journal of Advanced Manufacturing Technology*, *86*, 781–792.

Wang, D., Yang, Y., Liu, R., Xiao, D., & Sun, J. (2013). Study on the designing rules and processability of porous structure based on selective laser melting (SLM). *Journal of Materials Processing Technology*, *213*(10), 1734–1742.

Wang, Y., Xia, J., Luo, Z., Yan, H., Sun, J., & Lü, E. (2020). Self-supporting topology optimization method for selective laser melting. *Additive Manufacturing*, *36*, 101506.

Yap, C. Y., Chua, C. K., Dong, Z. L., Liu, Z. H., Zhang, D. Q., Loh, L. E., & Sing, S. L. (2015). Review of selective laser melting: Materials and applications. *Applied Physics Review*s *2*(4).

Yuan, M., Liu, Q., Liu, X., Kou, T., & Cui, Y. (2024). Study of the Effect of Selective Laser Melting Process Parameters on Overhang Structures. *Journal of Materials Engineering and Performance*, 1–17.

Yuan, Z., & Chen, X. (2023). Novel approach for fabricating horizontal overhanging structures in selective laser melting. Journal of Manufacturing Processes, 85, 793–801.

Zaeh, M. F., & Branner, G. (2010). Investigations on residual stresses and deformations in selective laser melting. Production Engineering, 4(1), 35–45.

Zhang, K., Fu, G., Zhang, P., Ma, Z., Mao, Z., & Zhang, D. Z. (2018). Study on the geometric design of supports for overhanging structures fabricated by selective laser melting. *Materials*, *12*(1), 27.

Zhang, X., Kang, J., Rong, Y., Wu, P., & Feng, T. (2018). Effect of scanning routes on the stress and deformation of overhang structures fabricated by SLM. *Materials*, *12*(1), 47.

BIOGRAPHICAL SKETCH

Prince Y. Asamani earned his bachelor's degree in Mechanical Engineering from Kwame Nkrumah University of Science and Technology in Ghana in 2019. Subsequently, he became a member of the Manufacturing and Industrial Engineering department at the University of Texas Rio Grande Valley, where he completed his Master of Science in Manufacturing Engineering in May 2024. During his time at the university, he contributed as a research assistant at the Center for Advanced Manufacturing and Cyber Systems (CAMICS), working closely with Dr. Benjamin Peters. Prince can be contacted via email at asamani.py1@gmail.com.